



MISSOURI  
**S&T**

# CENTER FOR TRANSPORTATION INFRASTRUCTURE AND SAFETY



## **Quality Control And In-Service Inspection Technology for Hybrid-Composite Girder Bridges**

by

Dr. Glenn Washer  
Associate Professor  
and

Justin Schmidt  
Graduate Research Assistant

Department of Civil and Environmental Engineering  
University of Missouri-Columbia

**NUTC  
R282**

**A National University Transportation Center  
at Missouri University of Science and Technology**

## ***Disclaimer***

The contents of this report reflect the views of the author(s), who are responsible for the facts and the accuracy of information presented herein. This document is disseminated under the sponsorship of the Department of Transportation, University Transportation Centers Program and the Center for Transportation Infrastructure and Safety NUTC program at the Missouri University of Science and Technology, in the interest of information exchange. The U.S. Government and Center for Transportation Infrastructure and Safety assumes no liability for the contents or use thereof.

**Technical Report Documentation Page**

1. Report No. NUTC R282		2. Government Accession No.		3. Recipient's Catalog No.	
4. Title and Subtitle Quality Control And In-Service Inspection Technology for Hybrid-Composite Girder Bridges				5. Report Date August 2014	
				6. Performing Organization Code	
7. Author/s Dr. Glenn Washer and Justin Schmidt				8. Performing Organization Report No. Project #00035268	
9. Performing Organization Name and Address Center for Transportation Infrastructure and Safety/NUTC program Missouri University of Science and Technology 220 Engineering Research Lab Rolla, MO 65409				10. Work Unit No. (TRAIS)	
				11. Contract or Grant No. DTRT06-G-0014	
12. Sponsoring Organization Name and Address U.S. Department of Transportation Research and Innovative Technology Administration 1200 New Jersey Avenue, SE Washington, DC 20590				13. Type of Report and Period Covered Final	
				14. Sponsoring Agency Code	
15. Supplementary Notes					
16. Abstract This report describes efforts to develop quality control tools and in-service inspection technologies for the fabrication and construction of Hybrid Composite Beams (HCBs). HCBs are a new bridge technology currently being evaluated by the Missouri Department of Transportation (MoDOT). The report includes analysis of the anticipated damage modes for the HCB members and suitable nondestructive evaluation (NDE) technologies that could be utilized for condition assessment. Infrared thermography (IR) was found to be the most applicable NDE technology for use in quality control/quality assurance (QC/QA) testing to ensure uniform placement of the concrete within the arch, which is critical to ensuring the quality of construction, durability, and capacity of the HCBs. Since this arch is enclosed within an FRP shell, internal voids or honeycombs that may occur during concrete placement are unavailable for visual inspection. It was found that the thermal signature of this arch, which results from the heat of hydration produced during the curing of the concrete, could be imaged on the surface of the composite shell. A procedure for utilizing IR technology to ensure the quality of the concrete placement in the arch was developed, tested and verified through field testing of each of the three HCB bridges constructed over the course of the project. This technology is also suitable for the detection of delamination in the composite shell. Recommendations developed from the research include: implementing thermal imaging technology as a QC/QA tool, utilizing visual inspection for the assessment of the composite shell in-service, and pursuing the application of Magnetic Flux Leakage (MFL) to assess corrosion damage in the strands. MFL technology is currently experimental in nature, and not readily available as a commercial tool. Development of this tool should be tracked in anticipation of future implementation.					
17. Key Words Hybrid-composite bridges, In-situ Monitoring, Load Testing, and Long-term Durability			18. Distribution Statement No restrictions. This document is available to the public through the National Technical Information Service, Springfield, Virginia 22161.		
19. Security Classification (of this report) unclassified		20. Security Classification (of this page) unclassified		21. No. Of Pages 49	22. Price

**QUALITY CONTROL AND IN-SERVICE INSPECTION TECHNOLOGY FOR  
HYBRID-COMPOSITE GIRDER BRIDGES**

---

Dr. Glenn Washer

Department of Civil and Environmental Engineering

Justin Schmidt, Graduate Research Assistant

## TABLE OF CONTENTS

ACKNOWLEDGEMENTS.....	ii
LIST OF FIGURES .....	iii
ABSTRACT .....	v
INTRODUCTION.....	1
POTENTIAL DAMAGE MODES FOR HCB.....	2
Voids In Concrete.....	2
Damage Modes for Shell Laminate .....	3
Steel Corrosion .....	5
NONDESTRUCTIVE EVALUATION TECHNIQUES .....	7
Ultrasonic Testing.....	7
Acoustic Emission .....	9
Infrared Thermography.....	11
Tap Testing .....	14
Magnetic Flux Leakage .....	15
FIELD OBSERVATIONS .....	17
Bridge B0439 Arch Pour.....	18
Bridge B0410 Arch Pour.....	20
Bridge B0478 Arch Pour.....	22
RESULTS.....	23
Camera Procedure And Placement.....	23
Mock-up Testing.....	26
Quality Control Testing of the HCB .....	27
Timing of QC Imaging .....	29

Detection of Voids.....	31
Anomalies .....	33
In-Service Testing .....	36
CONCLUSIONS .....	38
Recommendations .....	39
References.....	40

## LIST OF FIGURES

Figure 1: Example of potential damage modes for HCB.....	3
Figure 2: Testing Setup for Ultrasonic Pulse Velocity for HCB. ....	9
Figure 3: Schematic diagram of IR emission from a HCB during hydration of concrete. ....	13
Figure 4. Magnetic Flux Leakage test schematic.....	16
Figure 5. MFL system components (A) and system deployed on a prestressed box girder (B). ....	17
Figure 6. Photographs of HCB mock-up.....	18
Figure 7. Photograph showing concrete rising through shear connectors and workers vibrating connectors to consolidate SCC. ....	20
Figure 8. Photograph showing vibrator and concrete placement for bridge B0410 HCB.....	21
Figure 9. Diagrams of voids in SCC arch of B0410. ....	22
Figure 10. A & B: Photographs of concrete pump truck (left) and spans 1 & 2 during concrete placement (right) for Bridge B0478.....	23
Figure 11. IR image of HCB length (left) and diagram of corresponding camera location (right). ....	25

Figure 12. Thermal image at normal angle to HCB (right) with diagram of corresponding camera location (right). .....	26
Figure 13. Photograph (left) and thermal image (right) of the mockup specimen showing concrete arch. ....	27
Figure 14. Example thermal image showing thermal signature of the arch during the hydration of concrete. ....	28
Figure 15. Example of IR image (left) and photograph of HCB (right) being placed in the field. ....	29
Figure 16. Thermal image illustrating how temperature contrast was determined. ....	30
Figure 17. Thermal contrast at surface caused by hydration of concrete during 48 hours after placement. ....	31
Figure 18. Composite thermal images of the West (A) and East (B) webs of beam 1, HCB B0410. ....	32
Figure 19. Composite thermal image of void in B0410 (A) and temperature variations (B) along the line shown in (A). ....	33
Figure 20. Images showing thermal "hot spots" typically observed following concrete placement. ....	34
Figure 21. Example of anomalies observed in the area of the arch one year during the night (left) and during the day (right). ....	35
Figure 22. Thermal images of B0439 20 months after concrete placement showing HCB at (A) 6 pm with thermal profile (B), and (C) 5 am with thermal profile (D). ....	37
Figure 23. Thermal contrasts over a 24 hour period for B0439, 20 months after placement of concrete arch. ....	38

## **ABSTRACT**

This report describes efforts to develop quality control tools and in-service inspection technologies for the fabrication and construction of Hybrid Composite Beams (HCBs). HCBs are a new bridge technology currently being evaluated by the Missouri Department of Transportation (MoDOT). The report includes analysis of the anticipated damage modes for the HCB members and suitable nondestructive evaluation (NDE) technologies that could be utilized for condition assessment. Infrared thermography (IR) was found to be the most applicable NDE technology for use in quality control/quality assurance (QC/QA) testing to ensure uniform placement of the concrete within the arch, which is critical to ensuring the quality of construction, durability, and capacity of the HCBs. Since this arch is enclosed within an FRP shell, internal voids or honeycombs that may occur during concrete placement are unavailable for visual inspection. It was found that the thermal signature of this arch, which results from the heat of hydration produced during the curing of the concrete, could be imaged on the surface of the composite shell. A procedure for utilizing IR technology to ensure the quality of the concrete placement in the arch was developed, tested and verified through field testing of each of the three HCB bridges constructed over the course of the project. This technology is also suitable for the detection of delamination in the composite shell. Recommendations developed from the research include: implementing thermal imaging technology as a QC/QA tool, utilizing visual inspection for the assessment of the composite shell in-service, and pursuing the application of Magnetic Flux Leakage (MFL) to assess corrosion damage in the strands. MFL technology is currently experimental in nature, and not readily available as a commercial tool. Development of this tool should be tracked in anticipation of future implementation.



# 1 INTRODUCTION

2 This report provides an evaluation and analysis of potential inspection challenges  
3 and suitable nondestructive evaluation (NDE) techniques to assess the experimental  
4 Hybrid Composite Beam (HCB). NDE methodologies assessed include ultrasonic  
5 testing(UT), acoustic emission(AE), thermography(IR), magnetic flux leakage (MFL) and  
6 tap testing. The overall goal of this research was to implement bridge innovations for  
7 reducing cost of bridge construction and maintenance. The experimental HCBs  
8 constructed as part of this project are aimed at achieving these goals. HCB technology  
9 is new to the state of Missouri and has very limited service experience elsewhere.  
10 Therefore, an evaluation of potential challenges and technologies for inspecting these  
11 bridges was needed. The objectives of this research were as follows:

- 12 • Develop methods for quality control / quality assurance testing
- 13 • Evaluate potential serviceability and maintenance challenges

14 To achieve these objectives, an analysis of the potential damage modes that  
15 could affect these bridges was conducted. Potential damage modes include flaws or  
16 defects that may occur during the fabrication of the HCB members, as well as in-service  
17 damage modes that may occur during the service life of the bridge. Damage modes  
18 were identified and are described herein. A survey of available inspection technologies  
19 was also conducted to identify tools that could be used to assist in quality control (QC)  
20 and quality assurance (QA) testing. The NDE tools identified were focused on QC/QA  
21 testing of the concrete arch, which may be placed in a fabrication yard or in the field at  
22 the bridge site. Tools suitable for in-service inspection of HCBs are also discussed.

23 QC/QA testing of the arch using thermography was conducted for each of the  
24 members constructed during the project for three HCB bridges. The procedure used for  
25 casting the arch was also observed, and a description of the casting process is included  
26 herein to document the process used for these experimental beams. These data are  
27 documented in anticipation of additional applications of the technology in the future and  
28 to record the process utilized in this initial application of the technology.

29           During the course of the research, thousands of images of the HCB members  
30 were captured using infrared cameras. A small subset of these images are included to  
31 explain the technology and describe the most significant results found in the research.  
32 Tap testing of the composite shell was also completed for one of the three HCB bridges  
33 constructed.

## 34 **POTENTIAL DAMAGE MODES FOR HCB**

35           To properly assess the suitable inspection technologies that could be applied for  
36 HCB, it was first necessary to consider the potential damage modes and deterioration  
37 mechanisms that could affect these members. The assessment of this information is  
38 focused on two time periods: during the fabrication of members, at which time NDE  
39 could have a role as a QC/QA tool, and through the service life of the bridge, when NDE  
40 could play a role in maintaining the safety and serviceability of a bridge. The damage  
41 modes considered were focused on those that are most likely to occur during the  
42 fabrication and service life of the bridge.

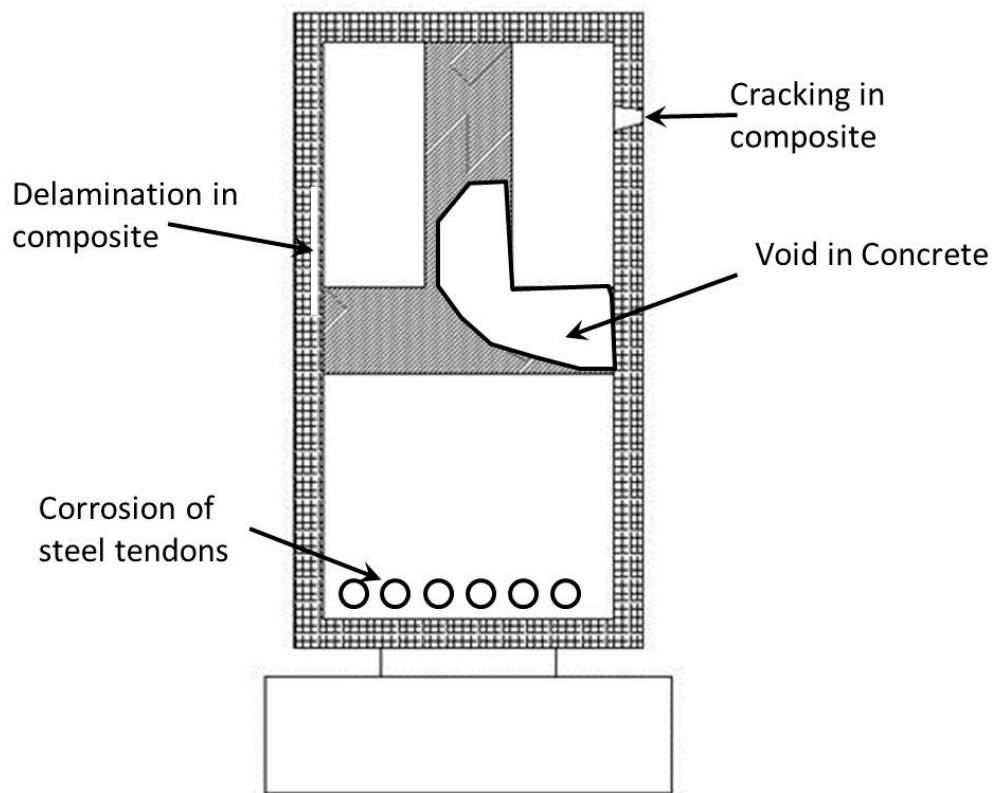
43           Figure 1 shows a schematic diagram of a HCB member to illustrate the  
44 anticipated damage modes. These include cracking of the composite shell surrounding  
45 the core, delamination in the composite shell, voids in the concrete, and corrosion  
46 damage in the prestressing strands that form the tie of the internal arch in the HCB  
47 members. Each of these damage modes is discussed in this section.

### 48 **Voids In Concrete**

49           Concrete is poured into the arch of the HCBs and acts as the compression chord  
50 for the member. Self-consolidating concrete (SCC) is used for casting this arch  
51 member. SCC typically has a higher flowability and workability than regular concrete.  
52 These characteristics improve SCC's ability to flow through forms and reinforcement  
53 and consolidate with limited or no vibration. The arch forms an important compression  
54 member for the HCB, and as such, voids or other discontinuities in the arch concrete  
55 may lead to reduced load capacity, increased deflections and long-term serviceability  
56 issues. As a result, it is important that this material be continuous and without  
57 significant voids resulting from improper placement of concrete.

58 Such voids, if they existed, are expected to be present following the concrete  
59 pour, and as such can be assessed during the construction phase and repaired if  
60 necessary. The internal concrete arch is contained within the FRP shell of the member,  
61 and polyiso foam is used to fill the HCB member and form the shape for the internal  
62 arch into which SCC is placed. Given the geometry of the section, voids are hidden  
63 from view by the composite shell and foam inserts, and as such these voids are not  
64 detectable through visual inspection at the time of construction.

65  
66



67  
68

Figure 1: Example of potential damage modes for HCB.

69

### 70 **Damage Modes for Shell Laminate**

71 There are two primary potential damage modes for the composite shell of the  
72 HCB - cracking of the shell and delamination between the layers of the shell. The  
73 potential damage mode of cracking, or breaking of the fibers, may result from loading

74 or overloading of the beam, the effects of fatigue loading, buckling of the compressive  
75 flange, or local flange or web buckling due to overloading [1, 2]. Generally, such a  
76 damage mode would progress to become surface-breaking and therefore can be  
77 observed through normal visual inspection.

78 The effect of ultraviolet radiation on the shell of the hybrid composite beam can  
79 increase the likelihood of cracking during the service life of the structure. Usually this  
80 cracking initiates as visual cosmetic damage in the surface resin of the shell which does  
81 not affect the structural properties of the FRP shell. This cosmetic damage includes  
82 surface color changes, loss of pigment, and loss of the surface luster of the laminate.  
83 Even though these damages are only visual cosmetic degradations in the surface resin,  
84 they can induce more significant damage in the shell [3, 4]. These degradations can  
85 eventually decrease the ultimate strain in the resin as well as decrease the specific  
86 toughness of the resin's surface layer. These decreases in the surface resin properties  
87 can cause the modulus of elasticity of the surface to increase and lead to crack  
88 propagation in the HCB shell.

89 Ultraviolet radiation damage to the shell of the HCB can be prevented through  
90 different additives in the resin formulas, or an application of a gel coat to the surface of  
91 the beam's shell. This gel coat is a thick resin layer on the exterior surface of the  
92 laminate which can be applied through spraying or rolling after the manufacturing of the  
93 beam. The gel coat also improves fire protection of the beam and provides an additional  
94 barrier against moisture[3]. Ultraviolet radiation damage is most likely to affect the  
95 fascia members of a bridge structure, particularly those facing the southern sky where  
96 solar exposure is anticipated. Generally, ultraviolet radiation damage to the composite  
97 can be observed visually, and affects the outermost layers of the fibers. Given that the  
98 composite shell only has a moderate role in the primary load paths in the structure, such  
99 damage is unlikely to be a significant safety concern over the service life of a HCB  
100 structure.

101 Delamination between the layers of the composite shell is also a potential  
102 damage mode. Delamination is likely to occur due to improper application of resin  
103 during the fabrication of the composite shell. Voids in the resin material or resin-starved  
104 areas may develop delamination[5]. Delamination has occurred in the lab testing of the

105 HCBs; however, this has only occurred during load testing that exceeds the factored  
106 demands[3]. The results of these tests are usually debonding of the web laminate from  
107 the interior polyiso foam core. Because this has occurred only when loading exceeds  
108 factored demands, and such a condition is unlikely for an in-service bridge,  
109 delamination of the composite shell has not been observed in the field.

110 Delamination can be detected using tap-testing methods or using infrared  
111 thermography (IR), as described later in the report. Since this damage mode is typically  
112 present at the time of fabrication, it can be appropriately addressed during QC testing.  
113 Localized delamination of the shell has only a modest effect on the load-carrying  
114 capacity of the composite material because shear transfer can be provided through the  
115 surrounding, well-bonded composite materials. As a result, delamination in the  
116 composite surrounding the HCB core is primarily a workmanship issue that can be  
117 addressed through the QC process.

118 Secondary potential damage modes were stated in the HCB Design and  
119 Maintenance Manual and are listed below with a short description of each [3]:

- 120 • Blistering: Identified as bumps in the surface, usually caused by a porous  
121 surface resulting from a poor gel coat application.
- 122 • Presence of Moisture: The laminates applied to the HCB shell are subject  
123 to moisture absorption. This can lead to degradation of the composite  
124 material
- 125 • Abrasion or Tearing: This type of damage may occur due to high water  
126 that results in debris impacting the composite or vehicles impacts below  
127 the bridge, which could result in section loss.
- 128 • Creep, Flow, or Rupture: These damage modes are of little concern due to  
129 the stiffness of the concrete and steel reinforcement, which creates low  
130 stresses and loads on the FRP laminates.

131 These secondary damage modes to the composite shell are generally available  
132 for assessment through visual inspection.

### 133 **Steel Corrosion**

134 Corrosion of the steel prestressing strands that form the tie in the HCB may be a  
135 longer-term maintenance concern. Because these strands are enclosed within the  
136 beam section, and hence unavailable for visual inspection, this damage mode will not  
137 be observable during normal, routine inspections. The steel strands are galvanized to  
138 provide a sacrificial material that will act as the anode in electrochemical corrosion

139 process. This will provide adequate corrosion protection in the near term. However,  
140 collection of moisture in the bottom of the HCB section where the steel is located could  
141 create a corrosive environment for the steel that corrodes the sacrificial zinc and leads  
142 to section loss. The box-like geometry of the HCB members is more likely to retain  
143 moisture than, for example, a member with an open section geometry. The box section  
144 may retain water in a manner similar to a voided slab bridge, where water collects in the  
145 voids despite weep hole that may be provided to prevent this from occurring. In the  
146 HCB members, pathways for water to enter to box section through the deck and  
147 concrete arch should be anticipated, based on past experience with voided slabs and  
148 adjacent box girder bridges.

149 Pitting corrosion in the steel strands is of particular concern. Localized areas of  
150 section loss, or pits, can develop such that the overall section loss may be nominal, but  
151 deep, localized pits reduce the tensile strength of the strand and result in strand  
152 fracture. Such localized corrosion damage may result from damage to the galvanizing  
153 during fabrication, from holidays in the galvanizing, or from localized degradation that  
154 penetrates the zinc layer.

155 An additional concern for galvanized strands stems from the fact that the tie  
156 chord is formed from high-strength prestressing strand. Such high-strength steel is  
157 susceptible to hydrogen-assisted cracking; high levels of hydrogen may be produced in  
158 the corrosion process for the zinc coating the strand, leading to hydrogen embrittlement  
159 of the prestressing strand, cracking or fracture of the wires, and subsequent reduction in  
160 load-carrying capacity.

161 Presently, there are no viable, commercially available and practical technologies  
162 for identifying strand fracture, with the possible exception of radiographic testing (RT).  
163 Field applications of RT are relatively rare for highway bridges due to the perceived  
164 health and safety concerns, and the practical constraints of testing in the field.  
165 However, magnetic technologies developed for the detection of section loss and strand  
166 fracture in prestressed beams offers a technology with potential for this application, and  
167 this technology will be discussed later in the report.

168 **NONDESTRUCTIVE EVALUATION TECHNIQUES**

169 This section of the report describes NDE technologies that may have application  
170 for QC/QA or in-service inspections of the HCBs. A survey of available NDE  
171 technologies was conducted with a focus on the assumed damage modes previously  
172 described. Those technologies most likely to provide suitable tools for the assessment  
173 of HCBs were down-selected for inclusion in this report. These include ultrasonic  
174 testing (UT), infrared thermography (IR), acoustic emission (AE), magnetic flux leakage  
175 (MFL) and tap testing.

176 **Ultrasonic Testing**

177 Ultrasonic testing has been in use as a nondestructive testing method for many  
178 years. Typically, ultrasonic tests are used to determine the thickness of a material or  
179 detect and evaluate the size of flaws and defects, such as corrosion, voids, and cracks.  
180 This NDE method utilizes sound wave propagation to conduct these measurements.  
181 During this project, ultrasonic pulse velocity measurements were considered as an NDE  
182 technology with the potential to be applied to the concrete arch for the detection of  
183 voids, honeycombs or poor quality concrete.

184 UT uses high frequency sound energy to propagate waves, normally ranging  
185 from 50 kHz to 50 MHz in frequency, through a material to conduct the testing. A UT  
186 system is typically comprised of two primary elements - a pulser/receiver and one or  
187 more transducers. The pulser produces a high voltage electrical pulse which acts on the  
188 transducer to create a pulse of acoustic energy, i.e an acoustic wave. The ultrasonic  
189 energy then propagates through the material, interacting with the composition of the  
190 material. If there is a defect in the material, or if the wave reaches the opposite side of  
191 the material, the wave is then reflected back to the receiver. The reflected wave portion  
192 is then transformed into an electrical signal to be displayed on the system's screen for  
193 data analysis.

194 Generally, smaller defects require shorter wavelengths to be detected, and as  
195 such higher frequencies are typically used, around 2-4 MHz. Larger defects typically  
196 require lower frequency, and longer wavelengths, around .5 to 2 MHz, to be detected.  
197 Due to these frequency requirements, higher frequencies (shorter wavelengths) are

198 used to test finer grained materials, such as metals, while lower frequencies (longer  
199 wavelengths) are used to test coarse grained materials, such as concrete. Increasing  
200 wavelength also increases the penetrating power of the wave, such that lower  
201 frequency waves can propagate over larger distances than high frequency waves. The  
202 rule of thumb for flaw detection using UT is that the wavelength cannot be larger than  
203 twice the size of the defect. Generally, frequencies of approximately 50 KHz are used  
204 for testing concrete, 2.25 MHz or greater is typically used for metals.

205 The primary limitation for UT is that a coupling medium is needed to transmit  
206 ultrasonic energy from the transducer into the material. As a result, direct access to the  
207 surface is required, and the surface must be adequately prepared such that coupling  
208 can be achieved. Additionally, because the ultrasonic energy is reflected at boundaries  
209 of the materials, layered materials present a particular challenge. The reflection  
210 coefficient, i.e. amount of energy reflected at a the boundary of the materials, can be  
211 determined from the relative acoustic impedances of the material involved; when  
212 acoustic impedance differences are high, the reflection coefficient is also high. As a  
213 result, very little ultrasonic energy is transmitted across the boundary.

214 A conceptual diagram of the setup for ultrasonic pulse velocity for a hybrid  
215 composite beam is shown in Figure 2. As shown in the diagram, the internal foam lies  
216 between the composite materials on the surface of the member and the concrete arch  
217 within the member. As a result, ultrasonic waves cannot be transmitted directly into the  
218 arch. Therefore this approach was considered ineffective for assessing the quality of  
219 the concrete arch.

220 UT can also be used to assess delamination in the composite material, through  
221 the use of surface waves propagating in the composite layer. Such technology has  
222 been previously demonstrated for use in aerospace vehicles and pressure vessels.  
223 However, such an approach is costly, time consuming and requires hands-on access to  
224 the entire surface of the composite material to be assess. Infrared thermography,  
225 described later in this report, is capable of detecting these delaminations without the  
226 requisite surface access necessary to implement ultrasonic technology. Consequently,  
227 UT for detecting delamination in the composite material was not pursued during the  
228 course of the research.



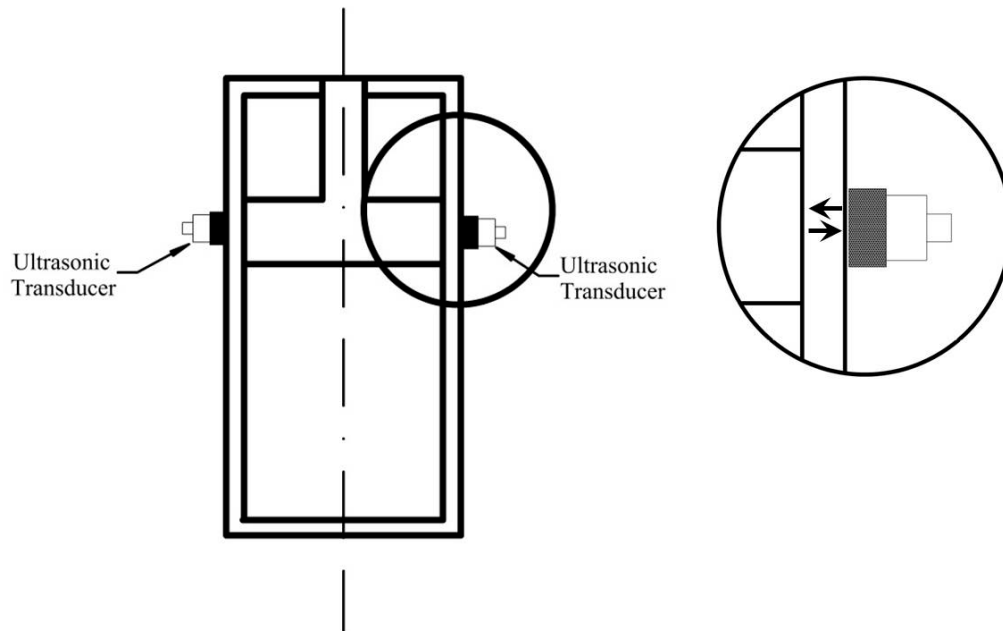


Figure 2: Testing Setup for Ultrasonic Pulse Velocity for HCB.

229  
230

## 231 **Acoustic Emission**

232 Acoustic Emission (AE) is a method of detecting the onset of damage in  
 233 materials based on burst of elastic energy associated with the formation of the damage.  
 234 The technique was first developed in the 1950's by materials scientists exploring the  
 235 formation of the microstructures in metals, and later developed as a means of  
 236 monitoring the development and propagation of the damage due to static and fatigue  
 237 loading [6]. Since that time, AE testing has become common for testing pressure  
 238 vessels, aerospace vehicles and other engineering applications. More recently, AE  
 239 methods have been developed exploring the application of AE as an NDE method for  
 240 concrete and concrete structures and composite materials.

241 The fundamental theory behind the generation of acoustic emissions in materials  
 242 is that propagation (growth) of a crack releases a small burst of elastic energy caused  
 243 by the extension of the crack surface on an atomic level, and plastic-zone development  
 244 processes surrounding the crack tip. This burst of elastic energy propagates as an  
 245 acoustic pulse through the material and can be detected by sensors coupled to the  
 246 surface of the material under test. For composite materials, cracking of the resin matrix

247 and fracture of individual fibers produce acoustic emissions that can be monitored as a  
248 means of evaluating damage induced during loading cycles.

249 The acoustic emissions are typically discriminated from other noise that may be  
250 present, such as traffic noise on a bridge, rubbing of bearings, etc., based on waveform  
251 characteristics[7]. Analysis of monitoring results typically consists of assessing the  
252 number of AE events per unit time, with increased AE activity being associated with  
253 crack nucleation and growth.

254 AE has traditionally been implemented for bridges as a monitoring technology,  
255 with a number of sensors placed permanently on a structure to monitor an area for  
256 incipient crack growth [8-10]. Typical applications include monitoring the AE activity of  
257 known cracks or assessing the effectiveness of a retrofit for arresting crack growth, as  
258 opposed to monitoring a bridge with no known cracks [11, 12]. Applications of AE for  
259 bridges comprised of composite materials has been very limited, although this  
260 technology is often used for composite-overwrapped pressure vessels during load  
261 testing[13]. Monitoring systems for AE testing typically consists of multichannel (16  
262 channels+) systems that can be mounted in the field and communicate data through  
263 phone lines or via cell phone connections.

264 The primary advantage of AE testing is the ability to monitor a large volume  
265 continuously, and to discriminate “active” damage, e.g. crack growth under load.  
266 Location of a defect can be assessed using multiple sensors on the material through  
267 cluster analysis and triangulation calculations.

268 One of the main disadvantages of AE is directly related to its main advantage.  
269 AE typically detects defects or damage that is actively growing. Existing defects or  
270 damage that are inactive (i.e. not growing) typically cannot be detected, because they  
271 do not produce acoustic emissions. An exception to this is concrete with distributed  
272 cracking, for which acoustic emissions stemming from rubbing of the crack faces may  
273 be used to qualitatively assess the health of a concrete member[14].

274 AE is a feasible technology for long-term monitoring of the composite shell for  
275 HCBs. Monitoring of the concrete arch and steel strands using AE is infeasible, due to  
276 the foam core positioned between these elements and the accessible surfaces of the

277 member. AE signals generated from damage in the concrete arch or steel stands would  
278 be attenuated before reaching the surface, where sensors would typically be placed.

279 The composite shell plays only a modest role in the structural capacity of the  
280 HCB, and this composite shell is available for visual inspection to assess damage that  
281 may develop. Consequently, it was concluded that AE was not a beneficial technology  
282 to be pursued for the in-service condition assessment of the HCBs.

### 283 **Infrared Thermography**

284 Infrared (IR) thermography has been used for a number of years for the condition  
285 assessment of concrete decks[15]. This technology is based on the principle that heat  
286 conduction through a material is affected by the presence of defects or discontinuities in  
287 the material, and that this disruption of heat flow manifests in observable temperature  
288 variations at the surface of the material[16-18]. These variations in surface temperature  
289 can be observed and recorded with IR cameras, which image the IR energy emitted  
290 from the surface.

291 IR cameras detect the electromagnetic radiation emitted from a body, which is  
292 proportional to the fourth power of the temperature of the body. All materials emit  
293 radiation in the infrared range when their temperature is above absolute zero (-273 °C).  
294 IR cameras are used to infer temperature of a material by measuring the  
295 electromagnetic radiation emitted or reflected from the surface [19]. The power of  
296 emitted radiation can be expressed by the Stefan-Boltzmann equation:

$$297 \quad E = \varepsilon\sigma T^4 \quad (1)$$

298 Where E is the radiant energy emitted by a surface at all wavelengths,  $\varepsilon$  is the  
299 emissivity of the materials,  $\sigma$  is the Stefan-Boltzmann constant ( $5.67 \times 10^{-8} \text{ W}/(\text{m}^2\text{K}^4)$ )  
300 and T is the temperature in degrees Kelvin. The emissivity of an object is a relative  
301 measurement of rate at which the object emits radiation, 1 being a perfect emitter and 0  
302 being no emission at all. In general, materials that are most common among civil  
303 structures, such as concrete, wood and asphalt pavement all have relatively high  
304 emissivity, between 0.9 and 1.0. The composite wrap surrounding the HCB core is  
305 expected to have a similar emissivity. The emissivity is a surface property, such that

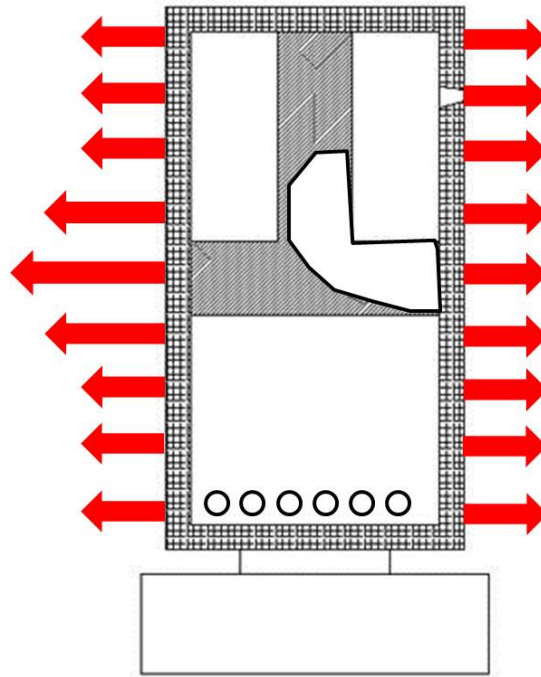
306 changes in the surface of the material as a result of debris, staining, oil, and water can  
307 influence the apparent temperature of the surface [17, 20].

308 For concrete structures, IR has traditionally been used for the detection of  
309 subsurface corrosion damage that results in delamination in the concrete. When a  
310 subsurface delamination exists in the concrete, it disrupts heat flow through the  
311 concrete. During the warming of the day, the area above the delamination warms more  
312 quickly than the intact concrete surrounding the delamination, resulting in increased IR  
313 energy being emitted from that area. During a cooling phase overnight, the concrete  
314 surface above a subsurface delamination will likewise cool at a faster rate than the  
315 surrounding concrete and appear as a cooler area in an infrared image [21].

316 However, for the HCB beams evaluated through this research, a different  
317 approach to thermal testing was evaluated. Following the placement of the concrete in  
318 the arch section of the member, the heat of hydration developed in the arch provides a  
319 significant heat source. If this heat source is sufficient, the thermal signature of the  
320 concrete arch could be apparent on the surface of the HCB. As shown schematically in  
321 Figure 3, this would result in increased emission of IR energy in the area of the arch,  
322 resulting in the observable signature on the surface that can be imaged using a thermal  
323 camera. This requires that the thermal energy be sufficient to penetrate approximately  
324 one inch of foam surrounding the arch, as well as the composite overwrap. If a void  
325 was present in the arch, the thermal energy from hydration would not be available in the  
326 area of the void. As a result, the thermal signature of the arch would not be apparent in  
327 thermal image of the surface. The approach of utilizing the heat of hydration for  
328 imaging subsurface features such as the arch has not been previously attempted, to the  
329 knowledge of the research team. However, if effective, this could provide a critical tool  
330 for QC testing of HCBs at the time of fabrication. This approach was evaluated through  
331 the course of the research and determined to be successful. Results will be described  
332 in the following sections.

333 If thermal images were not collected at the time of the fabrication of the member,  
334 the integrity of the concrete arch could also be evaluated in-service, provided that the  
335 thermal inertia of the concrete in the arch was sufficient. For such a scenario, the  
336 concrete arch would be thermally out of phase with the foam and composite that

337 surrounds it. This would result in the arch appearing cold during the early parts of the  
338 day, when environmental temperatures are increasing, and hot during the early evening,  
339 when environmental temperatures were cooling. Again, there is no prior experience  
340 with such an approach, but this approach was evaluated through the research and  
341 found to be successful.



342  
343 **Figure 3: Schematic diagram of IR emission from a HCB during hydration of concrete.**

344 One of the main advantages of IR testing is the ease of the testing procedure.  
345 The equipment is hand-held, and since it is a non-contact method, the testing can be  
346 performed at a distance. Access to the surface to be assessed is not required, and  
347 thermal images can be captured from distances of 100 ft or more. Therefore, testing  
348 can be done quickly and without disrupting traffic, construction, or any other process on  
349 site. For this project, thermal testing was the only technique used that could adequately  
350 detect the concrete through the FRP shell and polyiso foam core.

### 351 *IR Cameras*

352 Two different IR cameras were used to collect images during the course of the  
353 research. A FLIR S65 research-grade camera with a temperature sensitivity of 0.08 °C  
354 and an image size of 320 x 240 pixels was used to collect some IR images of the HCB

355 members during the early stages of the project. A FLIR T620 with a temperature  
356 sensitivity of 0.04 °C and an image size of 640 x 480 pixels was also used. The  
357 selection of the IR camera was based simply on the availability of the camera; either  
358 device has adequate capabilities to conduct the inspections.

## 359 **Tap Testing**

360 A simple method for searching for delamination and debonded areas is by  
361 mechanical sounding. Mechanical sounding is a method by which a metal or plastic  
362 object is used to strike the surface of the composite material. The tone produced by the  
363 impact is then analyzed; delaminated areas are identified by their distinctive hollow  
364 tone. This method can also be used to find delamination in concrete and debonding  
365 between concrete repair materials and the original concrete.

366 Sounding has been implemented for aerospace structures utilizing a metal coin  
367 (e.g. a quarter), and is commonly referred to as a coin-tap test. The low mass of a coin  
368 results in a high-pitched tone that can reveal delamination between layers of composite  
369 and possibly between the composite and the bonded substrate. For deeper features, a  
370 larger mass should be used so that the depth of the material is excited by the tapping.  
371 For composite retrofits on civil structures, a rock hammer or other suitable impact  
372 device may be used, though care should be taken to avoid damaging the composite  
373 material. The use of hammers allows for detection of features further from the surface,  
374 but near-surface features such as delamination between layers of composites may be  
375 obscured. A ¼ in. to ½ in. steel rod, approximately 6 inches in length, can also be used  
376 effectively in civil retrofit applications. The advantage of using this type of device is that  
377 it is readily available, since it can be formed from a piece of rebar. It can also provide  
378 both a high-mass and low-mass impactor depending on the orientation of the rod when  
379 impact is made.

380 Tap testing was utilized in this project to test the composite shell for one of the  
381 HCB members. However, IR technology is also well suited to this application and, since  
382 thermal images of all of the surface areas of all of the members was planned, tap  
383 testing was not utilized otherwise. Additionally, tap testing requires hands-on access to

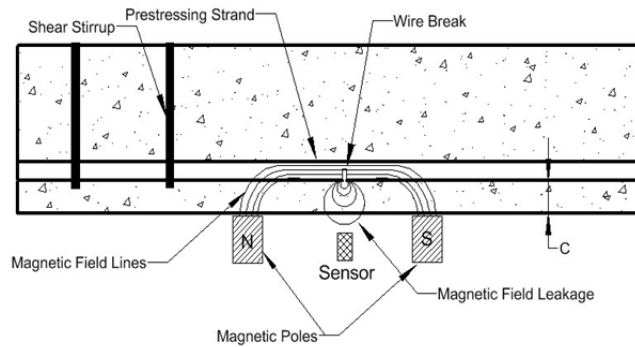
384 the entire area to be tested. As noted above, thermal imaging does not require this  
385 level of access, and is therefore more efficient and practical than tap testing.

### 386 **Magnetic Flux Leakage**

387 Magnetic flux leakage (MFL) is an NDE technology with the potential for  
388 detecting fractured prestressing strands embedded in concrete, and it has been a topic  
389 of research for several years[22, 23]. This technology may have application for  
390 condition assessment of the strands that form the tie of the HCB members

391 The MFL method works by inducing a magnetic field within the prestressing steel  
392 strand and detecting the leakage of that field that results from sudden discontinuities in  
393 the strand (i.e. fractured strand or section loss)[24]. The process of damage detection  
394 in the strand is analogous to the process involved in magnetic particle testing (MT). For  
395 MT, finely divided iron particles are attracted to magnetic fields leaking from a crack in  
396 the surface of the steel. For MFL, the leaking magnetic fields are detected using coils,  
397 Hall effect or SQUID (superconducting quantum interference device) sensors [25, 26].  
398 The leaking field can be detected through significant air gaps or concrete cover;  
399 detection through concrete cover of up to 11 inches have been reported in the literature  
400 [23, 27]. For the case of an HCB, the composite overwrap and the polyiso foam are  
401 diamagnetic materials that will behave similarly to air or concrete cover. As such, an  
402 MFL technology developed for detection of damaged strand in prestressed girders could  
403 also be applied to the HCB.

404 The method, as applied for a prestressed beam, is shown schematically in Figure  
405 4. Rare earth magnets are typically used to provide opposing magnetic poles. These  
406 poles are separated by a certain distance such that the magnetic field between the  
407 poles penetrates the concrete to induce magnetization in the embedded steel strand.



408

409

**Figure 4. Magnetic Flux Leakage test schematic.**

410

A sensor is used to measure the ambient magnetic field level at its position between the magnetic poles. The sensors and magnets form a sensor head that is scanned across the surface of the concrete axially aligned with the embedded steel strand. Sudden changes in the geometry of the embedded steel, such as a broken wire, result in a sudden change in the ambient magnetic field as the sensor head is scanned along the surface [28]. Changes in the cross-sectional area of the steel within the aperture of the sensor head also results in variations in the ambient magnetic field levels. These changes are less localized in nature relative to the response created by a fractured strand. Mild steel, such as steel stirrups, also results in variations of the ambient magnetic field and this complicates the interpretation of results [28]. Varying concrete cover can also create variations in the measured ambient field. However, even with these recognized limitations, the MFL approach provides a potential solution to nondestructively detecting broken and corroding strands embedded in concrete, and may also provide a technology for assessing the prestressing strands that form the tie of the HCB

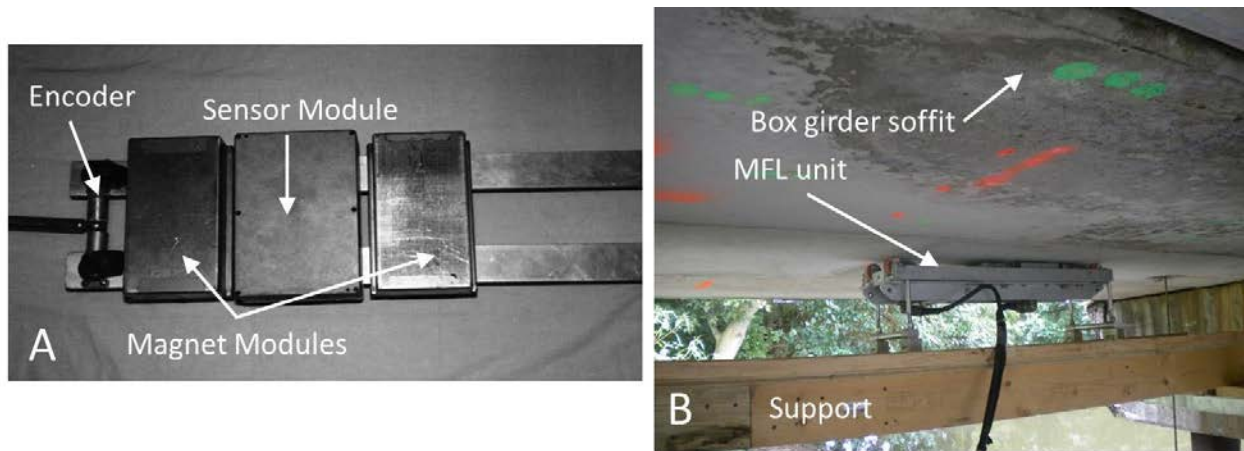
425

An example of the current state of the technology is shown in Figure 5. This figure shows a MFL unit developed at the University of Wisconsin [23]. Figure 5A shows a plan view of an MFL unit; Figure 5B shows the orientation of an MFL unit in use on the soffit of a box girder bridge. As shown in Figure 5A, the sensor head unit is comprised of two magnet modules, a sensor module, and an encoder that tracks the position of the unit as it is scanned along the length of the member. Magnetic field levels are monitored as the unit changes position along the member as shown in Figure 5B.

432



433 Research in the U.S. has typically focused on measuring the leakage field  
434 resulting from direct induction, i.e. during magnetization. An alternative approach is to  
435 utilize remnant or residual magnetization resulting from magnetizing the embedded  
436 steel. Electromagnetics are used to magnetize the embedded steel from distance up to  
437 ~12 inches [27]. The resulting magnetization of the embedded steel, which remains (at  
438 a reduced level) after the electromagnet is removed, creates a dipole in the area of a  
439 fracture of the strand or wire [24, 27]. Some research has suggested this method is  
440 more effective than induced magnetic fields; however, comparison data is limited.  
441



442  
443 **Figure 5. MFL system components (A) and system deployed on a prestressed box girder (B).**

444 Currently, MFL technology is not sufficiently developed to have been evaluated  
445 during the course of this research. The technology is experimental in nature, with the  
446 only systems available being research prototypes developed at the University of  
447 Wisconsin. However, in the longer term, such a technology may provide an important  
448 tool for detecting damage in the steel strands that form the tie of the HCB.  
449

## 450 **FIELD OBSERVATIONS**

451 This section of the report will describe the field observation of the procedures  
452 used for placement of concrete for each of the three HCB bridges constructed during  
453 the course of the project. During the course of the project, researchers attended each  
454 of the three casting procedures for the concrete arch to observe the procedure used to

455 cast the arch, and to evaluate the application of IR as a QC/QA tool. The research  
456 team also revisited bridges in-service, to evaluate that application of the thermal testing  
457 to the in-service beams. The results of these tests will be presented in later sections of  
458 the report. Tap testing of FRP shells for one of the bridges was completed to evaluate  
459 this technology. However, there were no defects identified during the tap testing. Since  
460 the method is comprised of striking the surface and listening to the tone produced, there  
461 are no results to present.

### 462 **Bridge B0439 Arch Pour**

463 The pour for the first set of hybrid composite beams for bridge B0439 took place  
464 over a one week period in August 2011. The pour site was in Mountain Grove, MO,  
465 located about one mile from the concrete plant. The procedure covered multiple steps.  
466 First, since HCBs are a fairly new procedure and technology for bridge construction in  
467 Missouri, a mock pour was scheduled the week before to practice the pour procedure. A  
468 wooden box served as the HCB shell, with one wall consisting of see-through Plexiglas  
469 in order to see if the procedure would allow the concrete to fill the entire arch. The  
470 mockup, shown in Figure 6, was one half of the length of the actual HCB, since the  
471 concept was to have concrete pushing itself down from the middle of the arch until the  
472 end block and entire arch were both filled completely. The same foam that was used in  
473 the HCBs was used in the mock up as well. The procedure proved to be successful in  
474 the mockup with the arch and end block completely filled. Some of the self  
475 consolidating concrete (SCC) did seep through the foam, but the arch remained intact  
476 without any voids visible through the Plexiglas wall.



477  
478 **Figure 6. Photographs of HCB mock-up.**

479

480           During the B0439 pour, only one concrete truck was used to deliver the SCC to  
481 the pour site; therefore it took an average of 45 minutes from the end of one beam pour  
482 to the beginning of the next. Once the concrete mix for the SCC was deemed  
483 acceptable on site, the SCC was then poured into the HCBs' arches. The beams were  
484 placed together in pairs at the pour site, with enough space left in between the pairs to  
485 park a truck. The SCC was poured into the beams directly from the concrete truck, as  
486 shown in Figure 7. A funnel was used to aid in the pour from the truck into the HCBs'  
487 concrete arch. During much of the pouring process, workers were observed discarding  
488 chunks of concrete that had begun to solidify in the truck.

489           The procedure for placing the concrete was as follows: the concrete would first  
490 be poured into one end hole until the end block was filled. The workers would then  
491 switch to the other end to fill in the opposite end block. The same procedure was used  
492 for the quarter holes, filling one then switching to the other, until finally concrete was  
493 poured into the center pour hole. This procedure would allow the concrete to keep  
494 pushing itself down until the arch was completely filled. This would become apparent  
495 on site due to concrete pushing up through the pour holes as well as through the shear  
496 connectors. To aid in the consolidation and flow of concrete through the arch, workers  
497 on site tried to use vibration on the concrete. To do this, workers would 'vibrate' the  
498 shear connectors sticking out of the top of the HCB, since these went down into the  
499 concrete arch. Workers would either hit the connectors with a hammer or shake them  
500 back and forth with their hands.



501  
502 **Figure 7. Photograph showing concrete rising through shear connectors and workers vibrating connectors to**  
503 **consolidate SCC.**

#### 504 **Bridge B0410 Arch Pour**

505 The pour for the second set of HCBs for bridge B0410 took place over a two  
506 week period in May 2012. Bridge B0410 consisted of three double web HCBs that span  
507 120 ft. The pour site was at a precast plant in Chesapeake, Virginia operated by  
508 Concrete Precast Systems.

509 The pour procedure for these double web HCBs generally followed the same  
510 process as that of B0439. However, there were some minor differences. For bridge  
511 B0410, the concrete was poured into the arches using a pump truck that was placed  
512 adjacent to the member. Different consolidating techniques were also used for the SCC  
513 in this bridge. A concrete vibrator was used to aid in concrete consolidation instead of  
514 vibrating the shear connectors. The vibrators were placed into the pour holes, along the  
515 top crevice where the shear connectors come out of the beam, and through some shear  
516 connector openings. These procedures can be seen in Figure 8 shown below.



Figure 8. Photograph showing vibrator and concrete placement for bridge B0410 HCB.

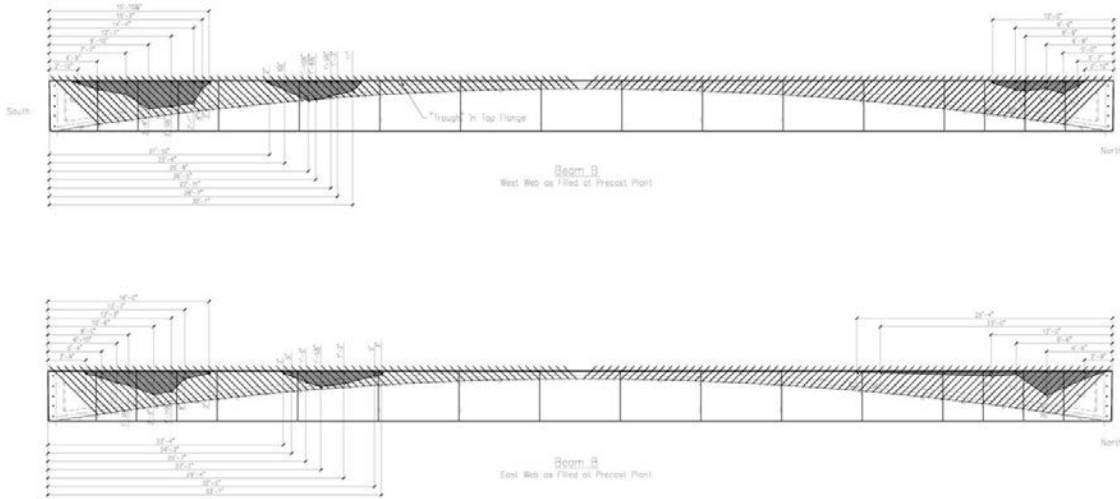
517  
518

519 Because B0410 consisted of double-web members, concrete could not be filled  
520 in one arch, or web, without counterbalancing it in the other. The pour was initiated at  
521 one end block, and once filled, the workers would move to the opposite end block on  
522 the other web and fill that end block. This simple procedure was to prevent the HCB  
523 from tipping over due to the weight of the concrete. The remaining end blocks were  
524 then filled. From there, the workers followed the same procedure, going from one  
525 quarter hole to the opposite web and opposite end quarter hole. When finished with the  
526 four quarter holes, the workers finished the pour with the two middle pour holes.

527 The pour for the bridge B0410 took two weeks to complete, due to weather  
528 conditions that included rain for a portion of the first week. One double web HCB was  
529 poured during the first week, while the remaining two were poured the second week.

530 During the pour of the first double web beam, it became apparent to workers and  
531 on-site quality control (QC) personnel that something had gone wrong with the concrete  
532 pour into the arch. Workers realized that the concrete was not rising as it should to the  
533 top of the arches inside the two webs. QC personnel then ran a simple test by sticking a  
534 ruler down through the shear connectors and pour holes to see if there were any voids  
535 in the concrete. A void map was then constructed from the information gathered and is  
536 shown in Figure 9. Voids were present in both arches and both ends of the beam.  
537 Additional concrete was poured into the arches through the shear connectors and  
538 additional pour holes drilled into the beam to fill the voids approximately one week after  
539 the original casting process. The voids were determined to be due to decreased  
540 flowability in the concrete at the time of the pour.

541



542

543

Figure 9. Diagrams of voids in SCC arch of B0410.

544

### 545 **Bridge B0478 Arch Pour**

546           The pour for the set of HCBs for bridge B0478 took place over two days in  
 547 August 2012. The pour site was the location of the bridge in Black, Reynolds County,  
 548 MO. The HCBs were delivered to the bridge site and placed on the abutments before  
 549 the pour. This was the only of the three bridges that had the concrete arch placed with  
 550 the HCBs placed in their final positions on the piers and abutments. Therefore, a pump  
 551 truck was required to pour the concrete into the arches since the bridge was already  
 552 erected, as shown in Figure 10. However, since the HCBs were single web beams, the  
 553 pour procedure more closely followed that of the first bridge, B0439. Multiple concrete  
 554 trucks were used to transport the SCC out to the bridge site in order to keep the  
 555 concrete pumping continuously.





556  
557  
558 **Figure 10. A & B: Photographs of concrete pump truck (left) and spans 1 &2 during concrete placement (right) for Bridge B0478**

559  
560 It should be noted that when pouring began on the first day, it was a goal that all  
561 12 beams were to be poured in the same day. However, delays were experienced as a  
562 result of difficulty with the quality of the SCC; as a result, the pouring procedure was  
563 extended into the second day.

## 564 **RESULTS**

565 This report will discuss the application of thermography as a QC/QA tool and as  
566 an in-service monitoring device. This technology has application for assessing voids in  
567 the concrete arch and delamination of the composite overwrap. During the course of  
568 the project, no delamination of the composite material was observed; consequently, this  
569 report focuses on the application of thermography for the assessment of voids in the  
570 concrete arch.

### 571 **Camera Procedure And Placement**

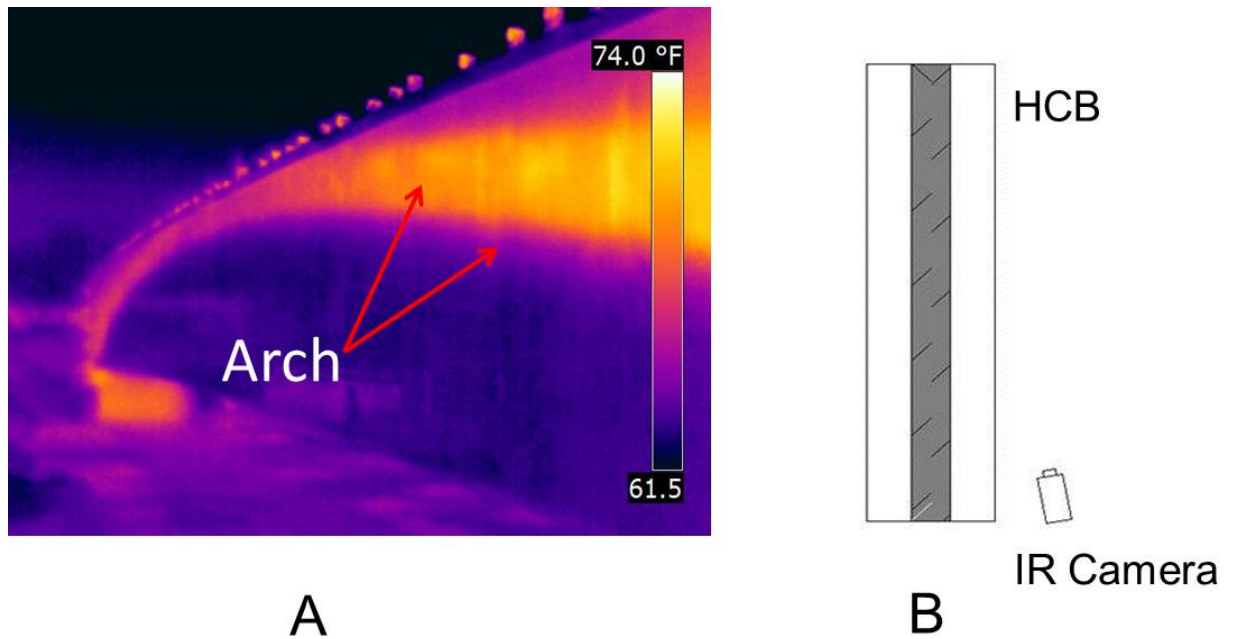
572 Throughout this project, thousands of thermal images of the three bridges were  
573 captured. To achieve the best results in the thermal images, certain procedures need to  
574 be followed. For example, the camera needs to be properly focused and appropriately  
575 oriented relative to the member being assessed. The best results are obtained with the  
576 camera oriented normal to the surface of the beam. During the course of the research,

577 this orientation was not always possible to do operational constraints that prevented  
578 appropriate access.

579 When access was limited to prevent a normal-angle image to be captured, the  
580 camera would be placed adjacent to the beam facing down the length of the member.  
581 This placement resulted in an isometric picture of the HCB, or, in other words, a picture  
582 of the length of the member at a low angle. Thermal images captured at such low  
583 angles typically exhibit a thermal gradient in the image that results from the variation in  
584 distance from the camera to the surface being imaged. This gradient results from the  
585 attenuation of the IR energy as it propagates through the air.

586 An example of an image captured at a low angle, along with a diagram of the  
587 camera's placement, can be seen in Figures 11 A & B. It can be observed in Figure  
588 11A that the surface of the member closest to the camera generally appears warmer  
589 than surfaces located far from the camera. This thermal gradient can compromise the  
590 quality of the thermal image and/or make interpretation difficult. The location adjacent  
591 to the beam was used on Bridges B0410 and B0478 because of the placement of the  
592 beams. For Bridge B0410, the pictures were taken at the pour site. The HCBs were  
593 placed very close together in order to make it easier on the pump truck during the  
594 pouring. Due to this location, the isometric pictures needed to be taken as there was no  
595 space available to place the camera at a normal angle with the surface of the member.  
596 For Bridge B0478, since the beams were placed on the abutments before the concrete  
597 was poured, access to position the camera at a normal angle was not possible.

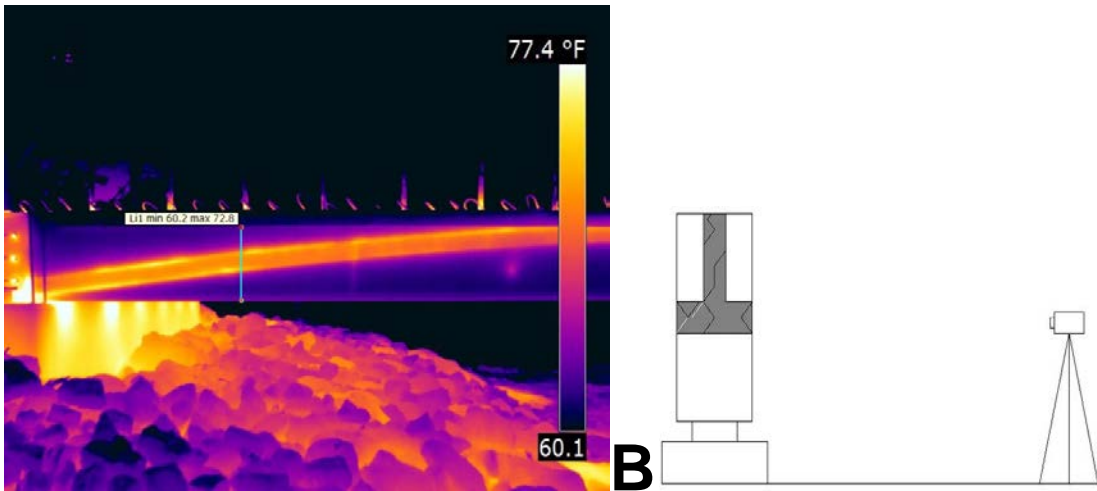




598  
599 **Figure 11. IR image of HCB length (left) and diagram of corresponding camera location (right).**

600 The preferred camera location was directly perpendicular, or normal, to the  
 601 surface of the beam. The camera was typically located about 10 to 15 feet away from  
 602 the beam at a normal angle with the surface of the member. This placement produced  
 603 an image of the full height of the beam, and without the thermal gradient typical of an  
 604 image captured at a low angle. An example of an image captured from the normal  
 605 position, along with a diagram of the camera's placement, can be seen below in Figures  
 606 12 A & B. This type of camera location was used whenever possible for all three  
 607 bridges.

608 The camera placement is an important consideration looking forward toward  
 609 implementing the IR technology as QC tool. To provide the best images, allocation of  
 610 adequate spacing for the camera to be position normal to the surface is required. When  
 611 the concrete arch is placed in a fabrication yard, this space can be provided by properly  
 612 positioning equipment and positioning the beams at an adequate spacing, typically 15 to  
 613 20 ft. apart. When casting of the arch occurs in-place at the bridge site, positioning the  
 614 camera to be most effective is more problematic, although images can still be captured  
 615 effectively, as shown in Figure 11.



616  
617  
618

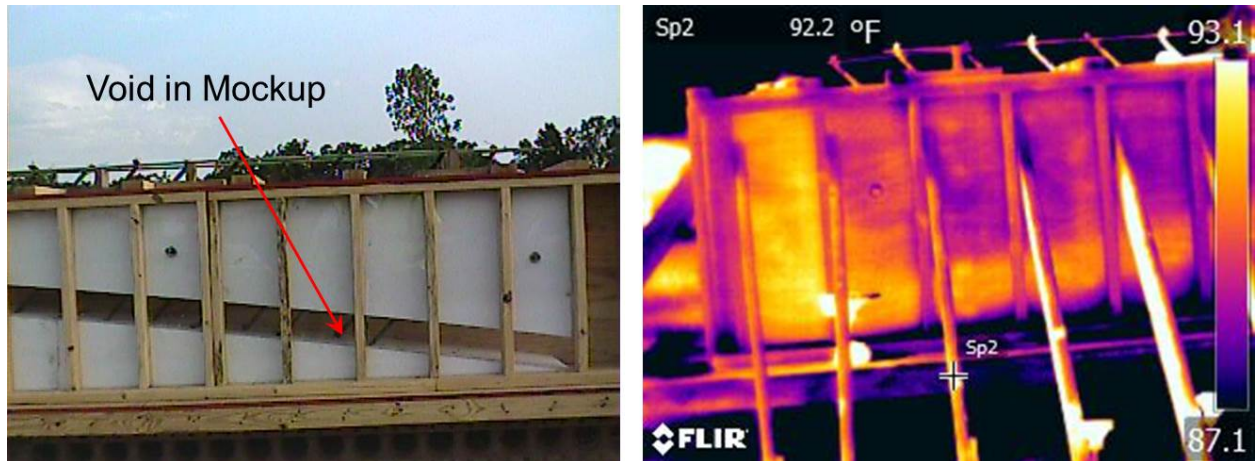
Figure 12. Thermal image at normal angle to HCB (right) with diagram of corresponding camera location (right).

### 619 **Mock-up Testing**

620 The mock-up of the HCB was tested using the S65 thermal camera as a proof of  
 621 concept test to establish if the proposed methodology for assessing the integrity of the  
 622 concrete arch was implementable. The forms for the mockup specimen consisted of  
 623 plexiglass and plywood, as discussed previously. It was found during the testing that  
 624 the thermal signature of the arch could not be imaged well through the Plexiglas wall of  
 625 the form. These materials are often opaque in the IR range, so this result was not  
 626 unexpected. Thermal images of the plywood wall of the form clearly showed the  
 627 thermal signature of the concrete following placement. Figure 13 illustrates a thermal  
 628 image of the concrete arch, along with a photograph of the mockup. Note that the  
 629 photograph of the mockup is taken from the side with a plexiglass wall, and shows the  
 630 void prior to concrete placement. The thermal image is taken from the opposite side of  
 631 the specimen, and as such has the opposite orientation.

632

633



634

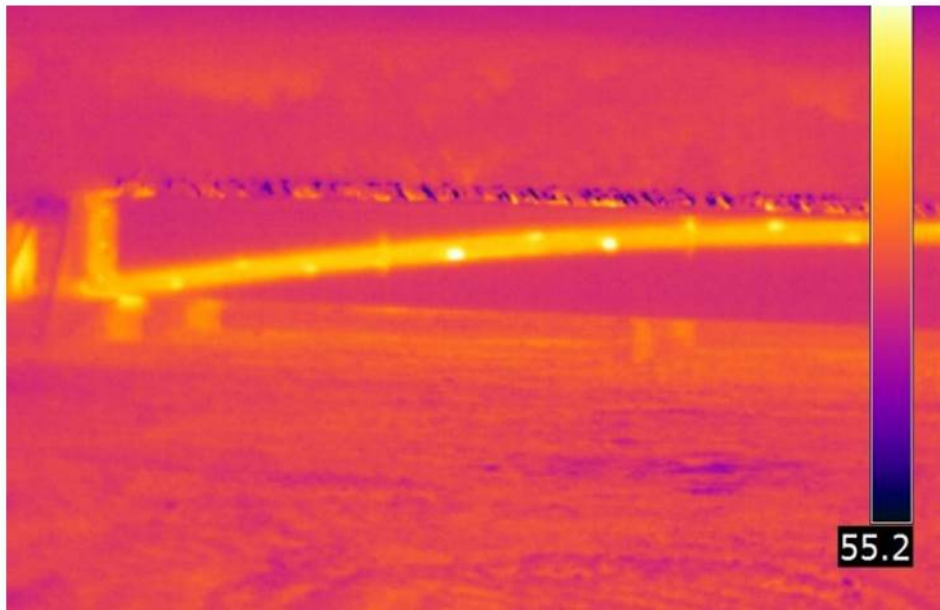
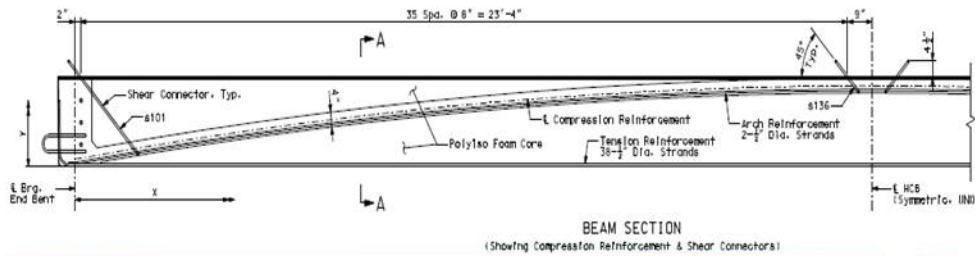
635 **Figure 13. Photograph (left) and thermal image (right) of the mockup specimen showing concrete arch.**

636 This initial test indicated that the concept of imaging the thermal signature of the  
637 concrete arch during the hydration of the concrete was a feasible approach. The  
638 general form of the concrete arch is apparent as a thermal contrast in the image,  
639 represented by different colors. This “thermal signature” of the concrete arch results  
640 from the heat of hydration of the concrete, as previously mentioned.

### 641 **Quality Control Testing of the HCB**

642 The application of the infrared thermography for QC testing of the HCB was  
643 demonstrated through the project. The procedure for acquiring IR data was to utilize a  
644 hand-held infrared camera to acquire data from a standing position adjacent to the  
645 HCB. A typical IR image is shown in Figure 14. This figure, which was acquired 24  
646 hours after the concrete pour, illustrates how the process works. As shown in the  
647 image, the heat of hydration of the concrete in the arch results in a thermal signature on  
648 the surface of the composite that images the internal arch. This thermal signature is  
649 revealed through the foam inserts and the composite wrapping that surrounds the arch.

650

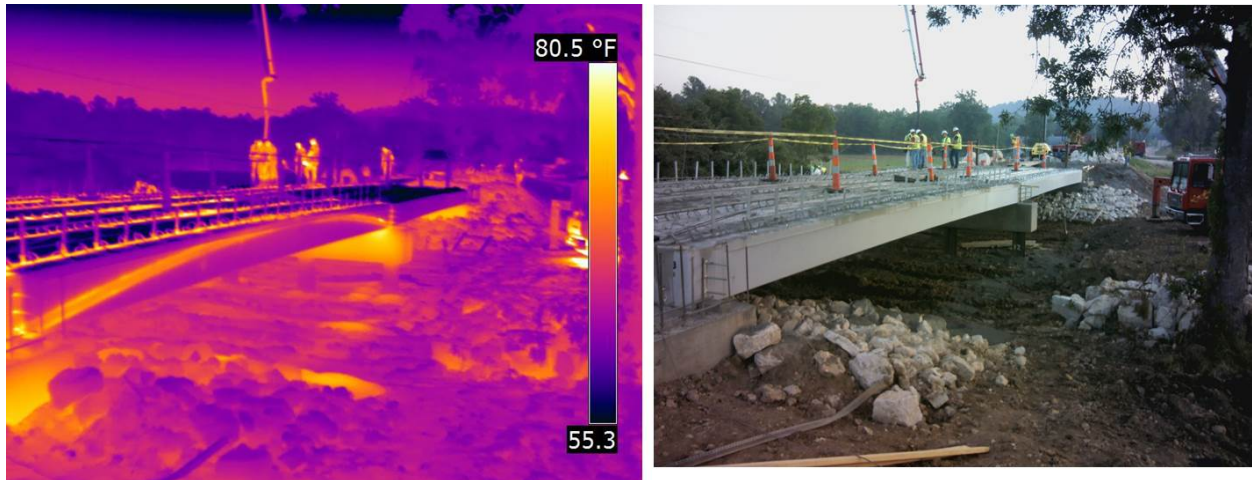


651  
652 **Figure 14. Example thermal image showing thermal signature of the arch during the hydration of concrete.**

653 Testing was completed during the fabrication of each of the three HCB bridges;  
654 testing was completed at the fabrication yard for two of the bridges, and for the third  
655 bridge testing was completed during the erection process as shown in Figure 15. In this  
656 figure, a span cast the previous day is imaged using the IR camera. Workers on the  
657 bridge shown in the photograph (Figure 15, right) are placing concrete on the next span.

658 Environmental conditions such as ambient temperature changes are typically a  
659 critical factor for imaging subsurface damage in concrete, such as corrosion-induced  
660 delamination. For QC testing of HCBs, where the heat of hydration of the concrete is  
661 creating the thermal signature of the arch on the surface of the composite,  
662 environmental conditions are much less critical. Because the arch is generating its own  
663 heat source it can be imaged regardless of the temperature conditions. Caution should  
664 be used in the case of rain, simply because the presence of water on the surface will  
665 obscure the thermal image.





666  
667 **Figure 15. Example of IR image (left) and photograph of HCB (right) being placed in the field.**

668 **Timing of QC Imaging**

669 A study was conducted to determine the optimum time for capturing images to  
 670 assess the concrete arch following concrete placement. Thermal imaging will be most  
 671 effective when the thermal contrast between the concrete arch signature and the  
 672 surface of the beam is greatest. Thermal images were captured at various times  
 673 ranging from 4 to 48 hours after concrete placement to assess this effect. The  
 674 temperature contrast was determine from the equation:

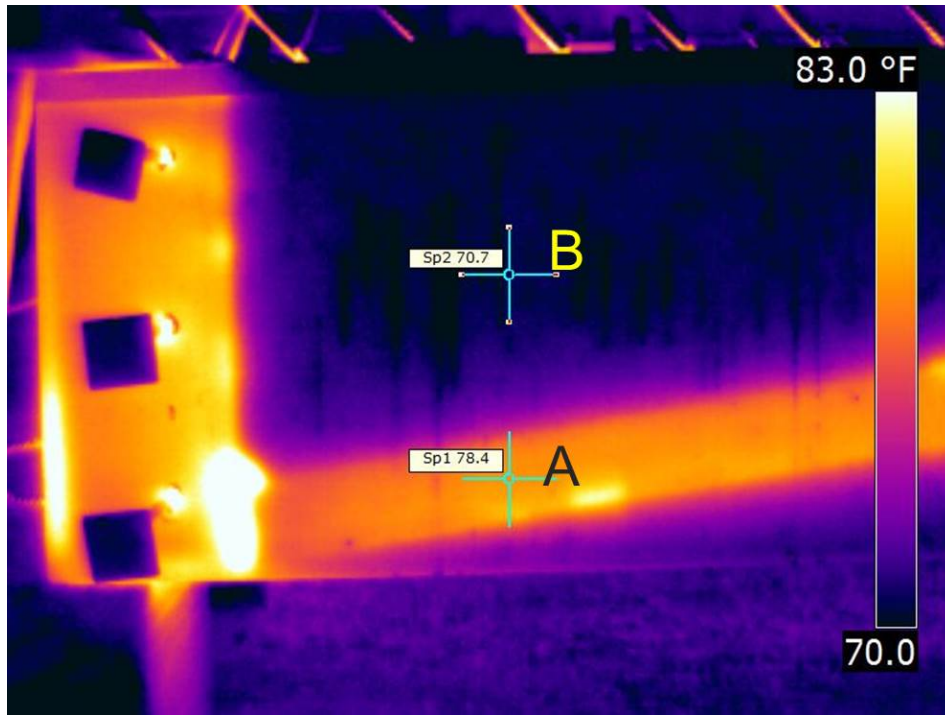
$$T_{contrast} = T_A - T_B$$

675 Where:

676  $T_A$  = Apparent temperature on the surface of the HCB above the concrete arch  
 677 and

678  $T_B$  = Apparent temperature on the surface of the HCB

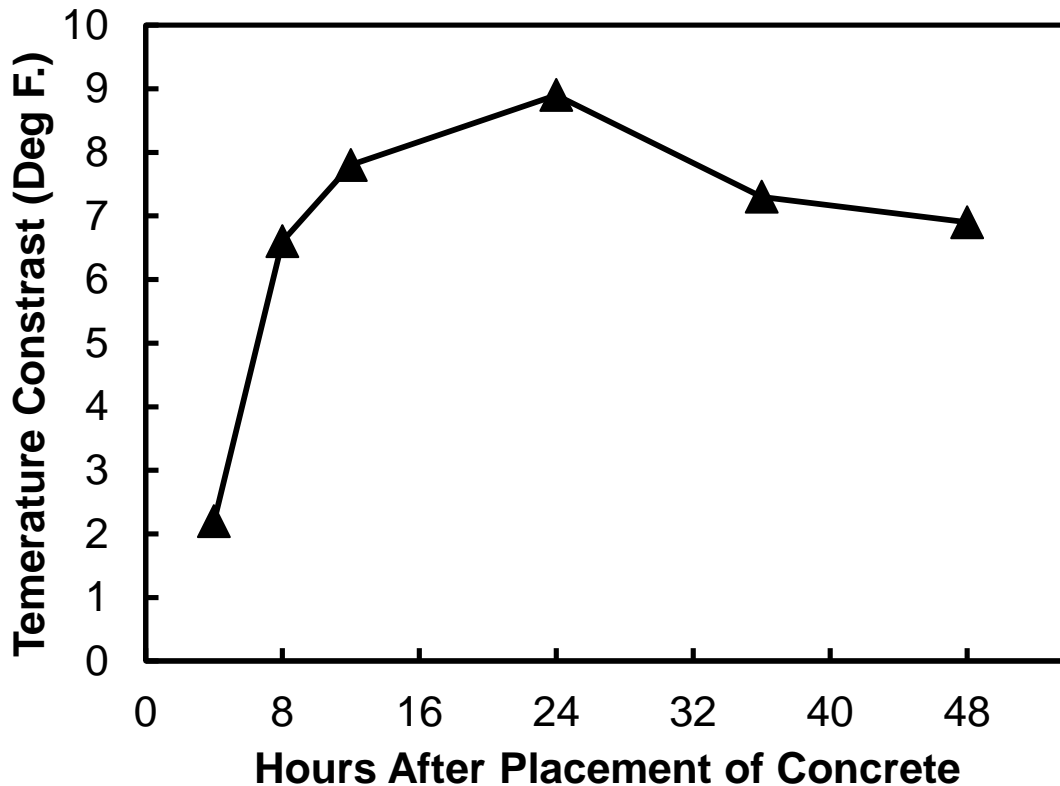
679 Figure 16 shows a typical location selected for calculating the temperature  
 680 contrast on the surface of the beam. This contrast was used determined to optimum  
 681 times for inspection. The thermal contrast can also be used to quantify the temperature  
 682 contrast developed from the hydration of the concrete or to quantify the contrast  
 683 resulting from ambient temperature variation once the hydration of the concrete is  
 684 complete.



685  
686

Figure 16. Thermal image illustrating how temperature contrast was determined.

687 Figure 17 shows the temperature contrast for the arch over a 48 hour time period. This  
688 figure represents the general behavior of all of the HCB's studied during the research,  
689 and shows that the optimum time for conducting an inspection for QC purposes is  
690 approximately 24 hours after the concrete is poured. The thermal contrast between the  
691 composite shell surface above the arch and other surface areas was almost 9 °F at this  
692 point in time. The thermal contrast was reduced at later measurement times. Images  
693 captured as late as 48 hrs after placement of the concrete still provided adequate  
694 thermal contrast to enable imaging of the concrete arch. From these data, the time  
695 period over which QC testing of the arch using IR should be conducted is approximately  
696 6 hours to 48 hours after the placement of concrete, with the optimum time being ~24  
697 hours after placement.

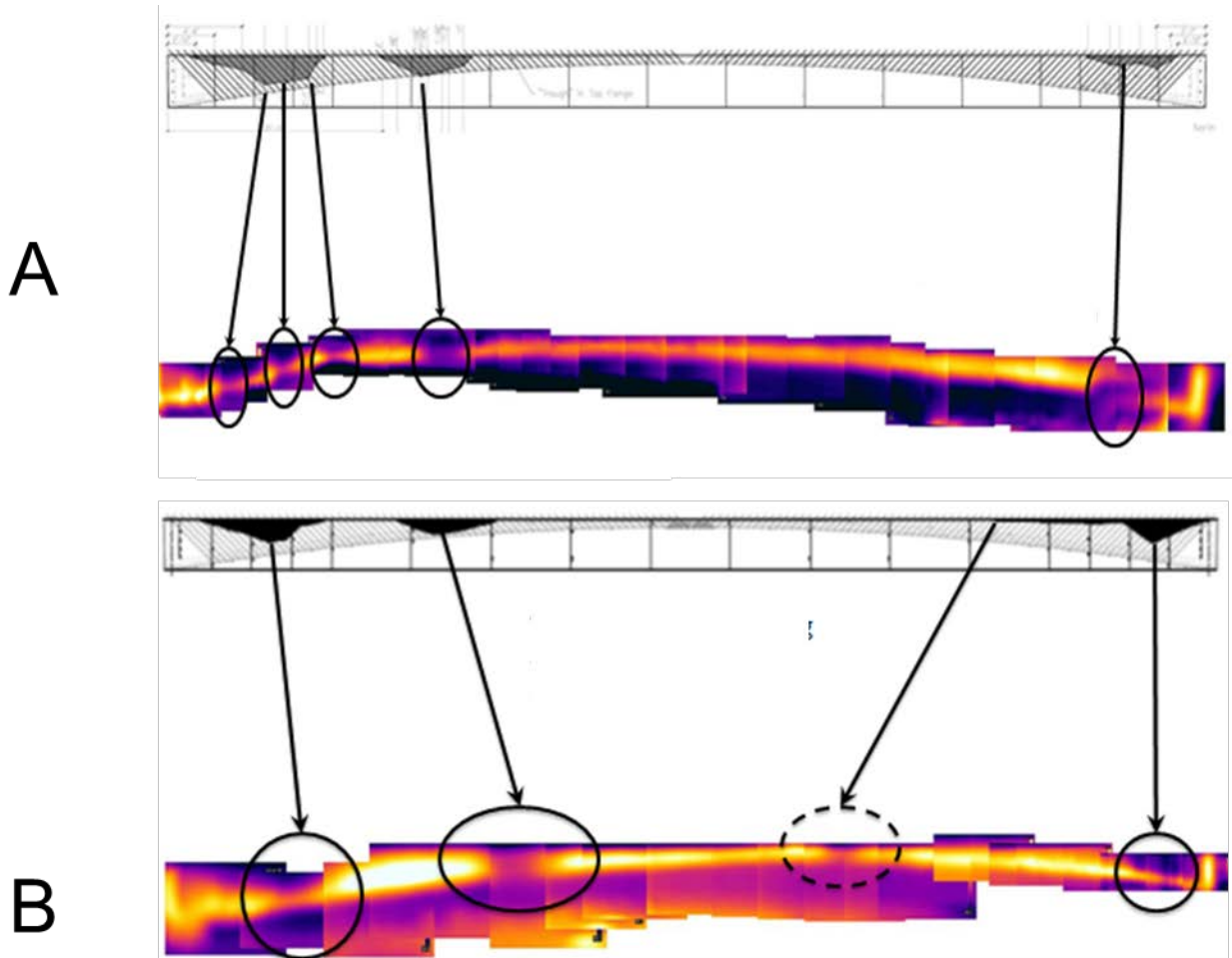


698  
699 **Figure 17. Thermal contrast at surface caused by hydration of concrete during 48 hours after placement.**

700 **Detection of Voids**

701 Thermal images were captured for each of the HCB bridges, typically 24 hrs and  
 702 48 hrs after the concrete placement. Generally, these images reveal an intact arch  
 703 producing a strong thermal signature on the surface of the HCB. However, during the  
 704 casting of Beam 1 of bridge B0410, the placement of the concrete resulted in several  
 705 voids in the concrete arches for each web of the member. These voids were apparently  
 706 caused by a lack of workability of the concrete, possibly due to the concrete beginning  
 707 its set prior to placement. The presence of the voids in the concrete arch was  
 708 recognized by the on-site QC personnel, because the concrete was not rising in the  
 709 forms in certain locations along the length of the girder. These voids were detected in  
 710 the thermal images captured 24 hours after the pour. Figure 18 illustrates the detection  
 711 of the voids in the thermal images, in a composite image formed by combining separate,  
 712 individual thermal images of portions of the beam. The blurriness of the images that  
 713 can be observed in Figure 18 was attributed to high humidity at the time the images  
 714 were captured. High humidity conditions can cause the auto-focus function of the

715 camera to not perform well. Regardless, the figure clearly shows the voids in the arch  
716 of the beam. Shown in the figure is the West web (A) and the East web (B) of the  
717 double – web HCB for bridge B0410. The void maps developed by on-site QC  
718 personnel is also shown to verify the thermal imaging results.

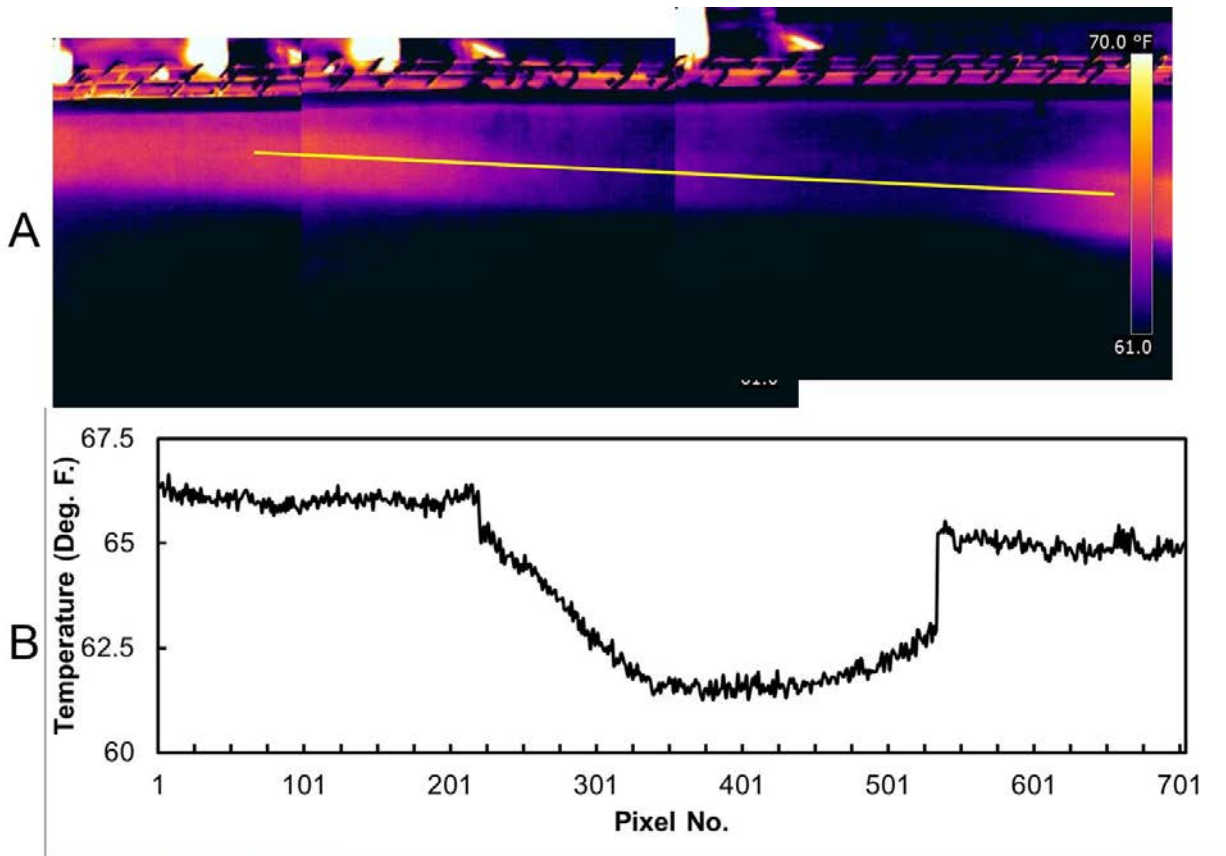


719  
720 **Figure 18. Composite thermal images of the West (A) and East (B) webs of beam 1, HCB B0410.**

721 The voids in the member result in the thermal signature of the arch disappearing  
722 at the locations of the voids. At these locations, the heat of hydration of the concrete is  
723 not available because the concrete is missing, i.e. there is a void. Figure 19 quantifies  
724 the thermal detection of one of the voids detected in this member, from data captured  
725 48 hrs after concrete placement. As shown in the figure, the signature of the concrete  
726 arch is not apparent in the thermal images; the temperature variations along a line  
727 shown in Figure 19A are shown in Figure 19B. The data presented in Figure 19B  
728 quantitatively illustrate the color variation in Figure 19A.



729



730

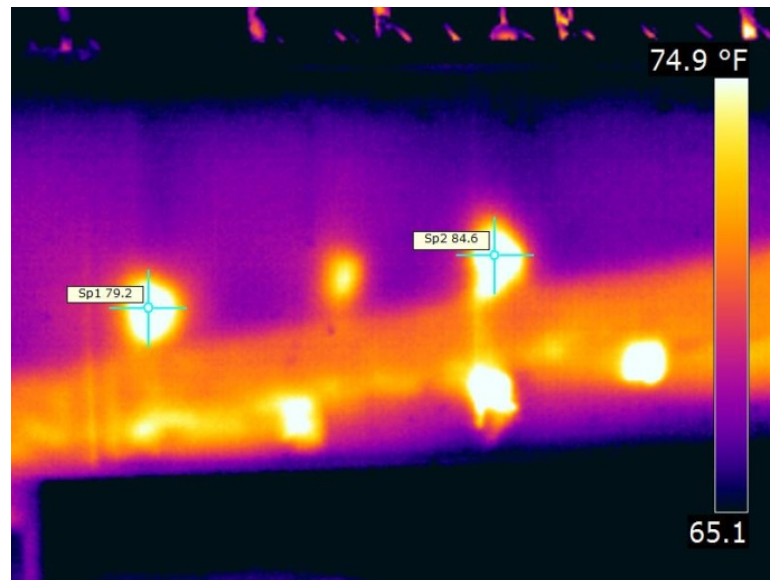
731 Figure 19. Composite thermal image of void in B0410 (A) and temperature variations (B) along the line  
732 shown in (A).

733 These figures clearly illustrate the ability of the IR thermography to detect the  
734 presence of voids in the arch, through the polyiso foam and composite overwrap that  
735 surrounds the arch. Given that this area is unavailable for visual inspection, this  
736 technology will provide an important tool for QC/QA testing at the time of casting of the  
737 arch, either in the field or in the fabrication yard. For the example shown here, the voids  
738 could also be detected from the top of the arch, however, voids or honeycombs may  
739 also occur without being apparent through the top of the member. The thermal method  
740 is an effective way to detect these voids.

#### 741 Anomalies

742 During the course of testing, there were a consistent pattern of anomalies  
743 appearing in the thermal images. These anomalies were represented by periodic “hot  
744 spot” appearing on the images, usually at locations on or near the surface above the

745 arch. Figure 20 illustrates some of the thermal anomalies observed. These “hot spots”  
746 may have resulted from the concrete placed in the arch void leaking through the polyiso  
747 foam, resulting in a larger thermal contrast reaching the surface of the composite shell  
748 in localized areas adjacent to the arch. These “hot spots” have greater thermal contrast  
749 than the arch itself, indicating that the heat of hydration is conducting across less  
750 material, that is, this is concrete that has pushed through the foam included in the HCB,  
751 and hence is closer to the surface. Leakage to the concrete through the foam inserts  
752 was observed during the mock-up testing, as noted previously.



753  
754 **Figure 20. Images showing thermal "hot spots" typically observed following concrete placement.**

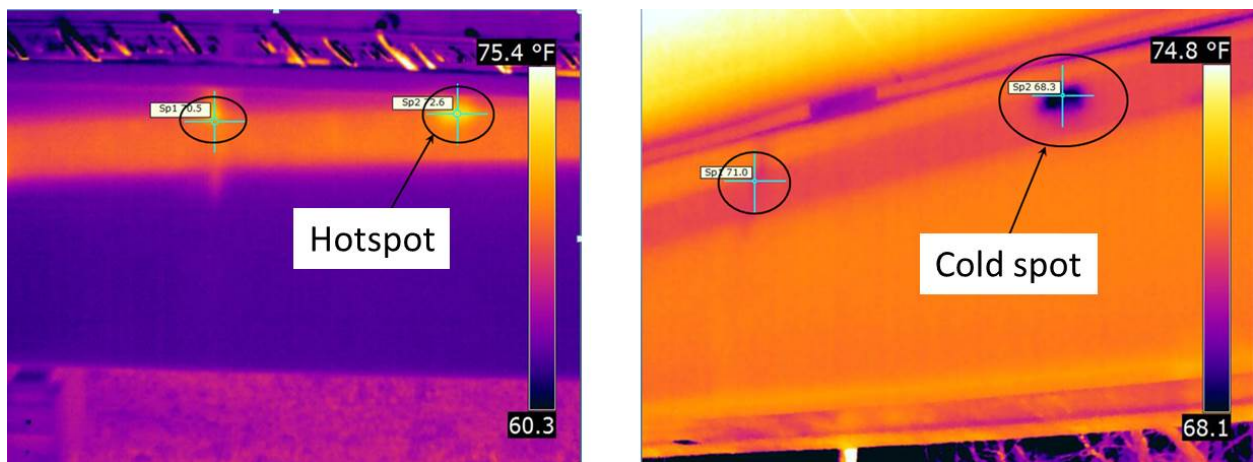
755 These anomalies were further assessed during testing 1 and 2 years after  
756 placement of the concrete. Figure 21 illustrates the locations of the anomalies one  
757 year after concrete placement for bridge B0439. As shown in these figures, the  
758 anomalies generally follow the thermal pattern of the concrete arch, that is, they are  
759 warmer during periods when the composite shell is cool, and cooler during periods  
760 when the composite shell is warm. This is likely due to the thermal inertia of the arch,  
761 which is out of phase with the variations in the surface temperature of the composite  
762 shell. As a result, these anomalies appear as “hot spots” during the nighttime, and “cold  
763 spots” during the warming cycle of the day. Thermal inertia or thermal mass,  $I$ , is a  
764 measure of the ability of the material to conduct and store heat. It is computed as the

765 square root of the product of thermal conductivity ( $k$ ), density ( $\rho$ ), and heat capacity  
766 ( $C_p$ ) as

767 
$$I = \sqrt{k\rho C_p}$$

768 Heat capacity (i.e. specific heat) is defined as the amount of heat needed to raise  
769 the temperature of a unit mass of a material by one degree. This property describes the  
770 ability of material to store heat. The volumetric heat of a material can be calculated as  
771 the product of the density and the specific heat of the material. It is a measure of the  
772 quantity of heat required to produce a unit temperature change in a unit volume [29].  
773 For the HCB, the significant thermal inertia of the concrete arch results in the  
774 temperature of the arch being out of phase with the surface temperature of the HCB in  
775 areas other than above the arch. These data indicate that these anomalies are part of  
776 the arch, i.e. this is concrete that has leaked through the foam to be in contact with the  
777 composite shell.

778 It is also possible that some of these thermal anomalies result from steel  
779 connection or fasteners that are in contact with the composite shell and embedded in  
780 the concrete, such that they follow the thermal pattern of the arch and conduct heat  
781 toward the surface of the composite shell. Regardless, these anomalies are not  
782 believed to be detrimental to the performance of the HCB.

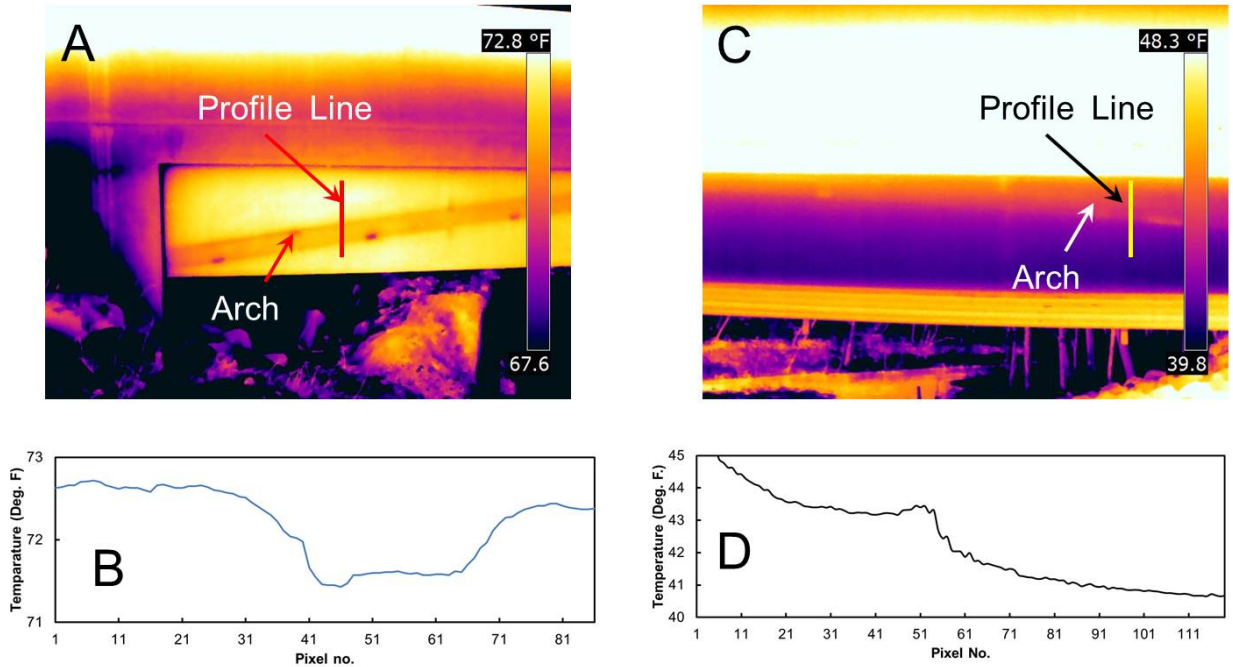


783  
784 Figure 21. Example of anomalies observed in the area of the arch one year during the night (left) and during  
785 the day (right).

786

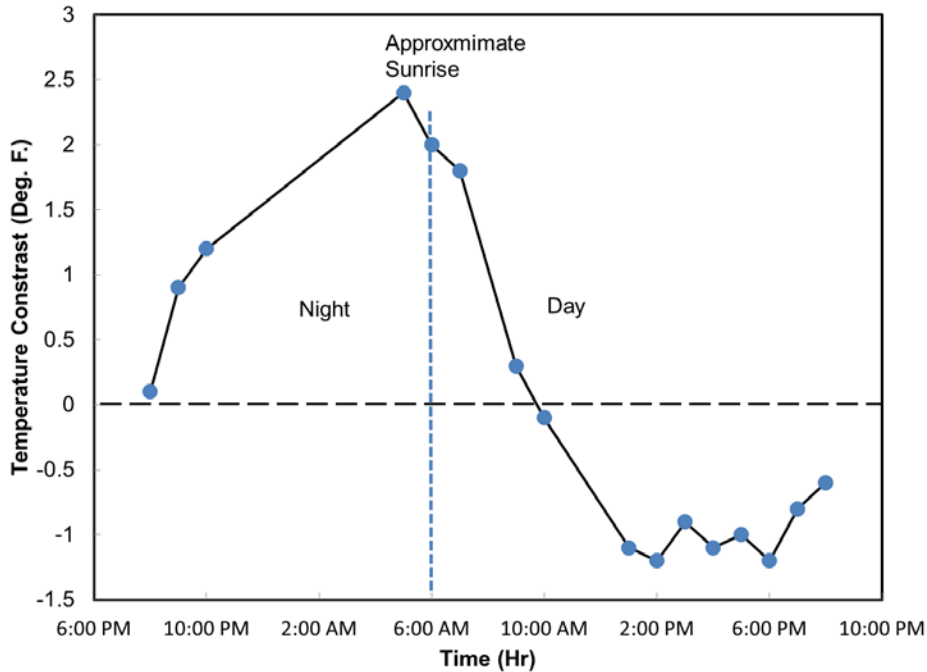
787 **In-Service Testing**

788 Thermal images of the HCBs were captured after the bridges were placed in-  
789 service, to assess if IR thermography could effectively image the arch after the  
790 hydration of the concrete was complete. The arch of Bridge B0439 was placed in  
791 August 2011. Thermal images were captured at the time of the casting, as well as in  
792 March 2012 (seven months after casting) and in April 2013. The results of these tests  
793 indicated that the concrete arch could be imaged after the hydration of the concrete was  
794 complete, due to the thermal inertial differences between the concrete arch and the  
795 surrounding foam and composite materials. Figure 22 illustrates the behavior of the  
796 concrete arch during the morning and evening hours. Figure 22 A shows a thermal  
797 image of the HCB at 6 pm in the evening, at which time the concrete arch appears  
798 cooler than the other portions of the HCB shell. The temperature gradient along the line  
799 shown in Figure 22A is shown in Figure 22B. The data in Figure 22B illustrate the  
800 actual temperature variation between the composite shell and the arch signature.  
801 Figure 22C shows an elevation of the HCB at 5 am in the morning. In this image, there  
802 is a significant gradient through the depth of the member, as illustrated in the gradient  
803 along the line shown in Figure 22D. This gradient results from the significant thermal  
804 energy stored in the concrete deck and parapets of the structure. Because these  
805 concrete elements store the thermal energy from the previous day, conduction of this  
806 thermal energy into the HCB results in the gradient shown. The gradient results in the  
807 arch signature being difficult to observe in the image, relative to the image captured at 6  
808 pm.



809  
 810 **Figure 22. Thermal images of B0439 20 months after concrete placement showing HCB at (A) 6 pm with**  
 811 **thermal profile (B), and (C) 5 am with thermal profile (D).**

812 The thermal contrast between the concrete arch signature and the composite  
 813 shell was monitored over a 24 hour period to determine the optimum times to conduct  
 814 an inspection for an in-service bridge. As shown in Figure 23, the greatest thermal  
 815 contrast between the concrete arch and the composite shell occurs in the early morning  
 816 hours, prior to sunrise. However, as noted above, the thermal images may be more  
 817 difficult to interpret at this time due to the thermal gradient along the elevation of the  
 818 member. It should also be noted that the behavior of the concrete arch is opposite of,  
 819 for example, a delamination in the composite shell would be. A delamination in the  
 820 concrete shell would be cold in the overnight hours, when that arch signature is warmer  
 821 than the surrounding area. During the day, a delamination would appear warmer than  
 822 the surrounding area. As a result, such a defect could be easily discerned from the arch  
 823 signature. There were no composite delamination defects observed over the course of  
 824 the project.



825

826

Figure 23. Thermal contrasts over a 24 hour period for B0439, 20 months after placement of concrete arch.

827

## CONCLUSIONS

828

The objectives of this research were as follows:

829

- Develop methods for quality control / quality assurance testing

830

- Evaluate potential serviceability and maintenance challenges.

831

These objectives were achieved in the research through a review of potential damage modes for the HCB members, an assessment of available inspection technologies, and the development of the appropriate NDE technology for QC testing of the concrete arch that forms a critical element of the HCB.

835

Damage modes for the HCBs included voids or lack of consolidation in the arch, damage of the HCB composite shell, and corrosion damage of the prestressing strands used as the tension tie in the arch. Voids or lack of consolidation in the arch was assessed using IR thermography. Methods for implementing IR thermography for detecting voids in the concrete arch were developed, tested and verified during the course of the testing. This technology successfully detected voids in the arch section during the casting of the arch for bridge B0410. The approach developed was

841

842 innovative and capitalized on the heat of hydration generated during the curing of the  
843 concrete. The IR thermography approach was demonstrated as an ideal solution for  
844 QC/QA of the concrete arch to detect voids in the concrete.

845         Damage modes identified for the HCB composite shell are generally available for  
846 visual inspection. Therefore, NDE technologies for this application were not pursued.  
847 However, the thermal methods used for assessing consolidation of the concrete arch  
848 are suitable for detection of delamination in the composite material. This technology  
849 can be applied as a QC/QA tool to assess the workmanship of the composite  
850 construction, or as an in-service inspection tool.

851         NDE technologies for the condition assessment of the prestressing strands are  
852 limited. Corrosion damage of these strands is an important long-term concern for the  
853 in-service performance of HCBs. Experimental methods based on MFL were described  
854 in the report. This technology is experimental at this time, and generally not available  
855 for practical bridge inspections.

## 856 **Recommendations**

857         Based on the research, the following recommendations are made:

- 858         1. Thermal imaging should be implemented as a QC/QA tool during the  
859             fabrication of the HCB bridges for the detection of voids in the concrete arch  
860             and delamination in the composite.
- 861         2. Visual inspection is a suitable tool for assessing the long term behavior of the  
862             composite shell
- 863         3. Progress on the development of practical tools for conducting MFL should be  
864             monitored, and this tool should be considered for monitoring of corrosion  
865             damage of the prestressing strand within the HCB members in the future.

866

867



868 **REFERENCES**

869

- 870 1. Karbhari, V.M., Chin, J.W., Hunston, D., Benmokrane, B., Justka, T., Morgan, R.,  
871 Lesko, J.J., Sorathia, U., Reynaud, D., *Durability Gap Analysis for Fiber-*  
872 *Reinforced Polymer Composites in Civil Infrastructure*. Journal of Composites for  
873 Construction, 2003: p. 238-247.
- 874 2. Hayes, M.D., *Structural Analysis of a Pultruded Composite Beam: Shear*  
875 *Stiffness Determination and Strength and Fatigue Life Predictions*, in *Engineering*  
876 *Science and Mechanics*. 2003, Virginia Polytechnic Institute and State University.
- 877 3. John R. Hillman, P., SE, *Hybrid-Composite Beam (HCB) Design and*  
878 *Maintenance Manual*. 2012: HCB, Inc. p. 37.
- 879 4. Karbhari, V.M., *Materials Considerations in FRP Rehabilitation of Concrete*  
880 *Structures*. Journal of Materials in Civil Engineering, 2001: p. 90-97.
- 881 5. Washer, G., Allempalli, S., *NDE Methods for Composite Materials*, in  
882 *International Handbook of FRP Composites In Civil Engineering*, M. Zoughi,  
883 Editor. 2013, Taylor and Francis: New York, NY.
- 884 6. Scott, I., *Basic Acoustic Emission*. Nondestructive Testing Monographs and  
885 Tracts. 1991, New York: Gordon and Breach Science Publishers.
- 886 7. Nair, A. and C.S. Cai, *Acoustic emission monitoring of bridges: Review and case*  
887 *studies*. Engineering Structures, 2010. **32**(6): p. 1704-1714.
- 888 8. Hutton, P.H., Skorpik, J. R., *Acoustic Emission Methods for Flaw Detection in*  
889 *Steel Highway Bridges*. 1978, Federal Highway Administration: Washington, D.C.  
890 p. 58.
- 891 9. Vannoy, D.W., Asmi, M., Liu, J., *Acoustic Emission Monitoring of the Woodrow*  
892 *Wilson Bridge*. 1987, Maryland Department of Transportatoin: Baltimore, MD. p.  
893 113.
- 894 10. Clemena, G.G., Lozev, M. G., Duke, J. C., Sison, M. F., *Interim Report: Acoustic*  
895 *Emission Monitoring of Steel Bridge Members*. 1995, Virginia Department of  
896 Transportation: Richmond, VA. p. 68.
- 897 11. Prine, D.W., Marron, D.R., *Acoustic Emission and Strain Gage Monitoring of*  
898 *Prototype Retrofit for Caltrans Structure B-22-26 R/L, I-80 Sacramento River*  
899 *(Bryte Bend), Sacramento, CA*. 1997, Infrastructure Technology Institute,  
900 Northwestern University: Evanston, IL.
- 901 12. Kosnik, D.E., Hopwood, T., Corr, D.J. *Acoustic Emission Monitoring for*  
902 *Assessment of Steel Bridge Details*. in *Review of Progress in Quantitative Non-*  
903 *Destructive Evaluation*. 2010. San Diego, CA: American Institute of Physics.
- 904 13. ElBatanouny, M.K., et al., *Identification of Cracking Mechanisms in Scaled FRP*  
905 *Reinforced Concrete Beams using Acoustic Emission*. Experimental Mechanics,  
906 2014. **54**(1): p. 69-82.
- 907 14. Gostautus, R.S., Tamutus, T., *Condition Assessment of Prestressed Concrete*  
908 *Girders From The Lakeview Drive (I-70) Bridge Using Acoustic Emission*, in  
909 *Western Pennsylvania Transportation Research Forum*. 2007: Pittsburgh, PA.
- 910 15. ASTM, *Standard Test Method for Detecting Delaminations in Bridge Decks Using*  
911 *Infrared Thermography*. Standard ASTM D4788 - 03(2007). 2007, ASTM  
912 International: West Conshohocken, PA, United States.



- 913 16. Manning, D.G. and T. Masliwec, *Application of Radar and Thermography to*  
914 *Bridge Deck Condition Surveys*. Bridge Management: Inspection, Maintenance,  
915 Assessment and Repair Papers Presented at the Second International  
916 Conference on Bridge Management, Held at the University of Surrey, Guildford,  
917 UK April 18-21, 1993, 1990.
- 918 17. Manning, D.G., and Holt, F.B., *Detecting Delaminations in Concrete Bridge*  
919 *Decks*, in *Concrete International*. 1980. p. 34, 41.
- 920 18. Maser, K.R. and W.M.K. Roddis, *Principles of Thermography and Radar for*  
921 *Bridge Deck Assessment*. Journal of Transportation Engineering, 1990. **116**(5):  
922 p. 583-601.
- 923 19. Bangalore, G.S., *Nondestructive evaluation of FRP composite members using*  
924 *infrared thermography*. 2002, West Virginia University.
- 925 20. Avdelidis, N.P. and A. Moropoulou, *Emissivity considerations in building*  
926 *thermography*. Energy & Buildings, 2003. **35**(7): p. 663-667.
- 927 21. Washer, G.A., *Application of Infrared Thermography (IR) for Detecting Defects in*  
928 *Concrete*. 2009, American Society for Nondestructive Testing.
- 929 22. Ciolko, A.T., Tabatabai, H., *Nondestructive Methods for Condition Evaluation of*  
930 *Prestressing Steel Strands in Concrete Bridges*, in *NCHRP Web Document*.  
931 1999, Transportation Research Board Washington, D.C.
- 932 23. Ghorbanpoor, A., Borchelt, R., Edwards, M., and Abdel Salam, E., *Magnetic-*  
933 *Based NDE of Prestressed and Post-Tensioned Concrete Members - The MFL*  
934 *System*, U.S.D.O.T., Editor. 2000, F.H.W.A.: Washington, D.C. p. 99.
- 935 24. Makar, J. and R. Desnoyers, *Magnetic field techniques for the inspection of steel*  
936 *under concrete cover*. NDT & e International, 2001. **34**(7): p. 445-456.
- 937 25. Krause, H.J., et al., *SQUID array for magnetic inspection of prestressed concrete*  
938 *bridges*. Physica C: Superconductivity, 2002. **368**(1-4): p. 91-95.
- 939 26. Ghorbanpoor, A., *Magnetic based NDE of steel in prestressed and post-*  
940 *tensioned concrete bridges*, in *Structural Materials Technology III: An NDT*  
941 *Conference*, R. Medlock, Chase, S., Editor. 1998, SPIE: San Antonio, TX. p. 343-  
942 347.
- 943 27. Scheel, H., Hillemeier, B., *Location of Prestressing Steel Fractures in Concrete*.  
944 *Materials in Civil Engineering*, 2003. **15**(3): p. 7.
- 945 28. Gaydecki, P., et al., *Inductive and magnetic field inspection systems for rebar*  
946 *visualization and corrosion estimation in reinforced and pre-stressed concrete*.  
947 *Nondestructive Testing & Evaluation*, 2007. **22**(4): p. 255-298.
- 948 29. Lienhard, J.H., *A Heat Transfer Textbook*. 2011, Mineola, N.Y.: Dover  
949 Publications.
- 950  
951